Exploring the composition and volatility of secondary organic aerosols in mixed anthropogenic and biogenic precursor systems

Aristeidis Voliotis[1], Yu Wang[1], Yunqi Shao[1], Mao Du[1], Thomas J. Bannan[1], Carl J. Percival[2], Spyros N. Pandis[3], M. Rami Alfarra[1,4], and Gordon McFiggans[1]

5   [1]Centre for atmospheric science, Department of Earth and Environmental Science, School of Natural Sciences, The University of Manchester, Oxford Road, M13 9PL, Manchester, United Kingdom

[2]NASA Jet Propulsion Laboratory, California Institute of Technology, 4800 Oak Grove Drive, Pasadena, CA 91109, USA.

[3]Department of Chemical Engineering, University of Patras, Patras, Greece

10   [4]National Centre for Atmospheric Science, Department of Earth and Environmental Science, School of Natural Sciences, The University of Manchester, Oxford Road, M13 9PL, Manchester, United Kingdom

Correspondence to: g.mcfiggans.manchester.ac.uk; aristeidis.voliotis@manchester.ac.uk

Abstract. Secondary organic aerosol (SOA) formation from mixtures of volatile precursors may be influenced by the molecular interactions of the products of the components of the mixture. Here, we report measurements of the

15   volatility distribution of SOA formed from the photo-oxidation *o*-cresol, *α*-pinene and their mixtures, representative anthropogenic and biogenic precursors, in an atmospheric simulation chamber. The combination of two independent thermal techniques (thermal denuder and the Filter Inlet for Gases and Aerosols coupled to a high resolution time of flight chemical ionisation mass spectrometer) to measure the particle volatility, along with detailed gas and particle phase composition measurements provides links between the chemical composition of the

20   mixture and the resultant SOA volatility. The products that were only present in the SOA of the mixture had higher O:C and lower volatility compared to those deriving from the individual precursors. This suggests that new product formation can reduce the volatility in mixtures. At the same time, some of the larger molecules with lower volatility produced in the single *α*-pinene and *o*-cresol system were not present in the mixture leading to an increase of the average volatility. These opposite effects resulted the volatility distribution of the SOA of the mixture to be between

25   those of the individual precursors. For example, compounds with effective saturation concentration less or equal than 0.01 μg m^{-3} represented 28, 39 and 37% of the SOA mass in the *α*-pinene, *o*-cresol and mixed precursor experiments, respectively. We further explore the sensitivity limitations of our technique to the reported results and we show that the particle volatility can be qualitatively assessed, while caution should be held when linking the chemical composition to the particle volatility. These results provide the first detailed observations of SOA particle

30 volatility and composition in mixed anthropogenic and biogenic systems and provides an analytical context that can be used to explore particle volatility in chamber experiments.

1. Introduction

Aerosol particles are ubiquitous in the atmosphere with substantial impacts on climate (Ramanathan et al., 2001)
35 and human health (Lelieveld et al., 2015;Brunekreef and Holgate, 2002). These particles may contain a wide variety of compounds, with the organic fraction contributing up to 90% of the mass in the submicron size range (Jimenez et al., 2009). The majority of this fraction is comprised by secondary organic aerosol (SOA) (Kanakidou et al., 2005;Hallquist et al., 2009;Shrivastava et al., 2017). SOA is formed by the oxidation of volatile organic compounds (VOC) in the atmosphere. These reactions result in a variety of products that can be more or less volatile than their
40 precursors depending on the underlying chemical processes in the gas and/or condensed phase (Donahue et al., 2012). The less volatile products of these reactions tend to partition to pre-existing particles and/or nucleate to form new particles. SOA containing particles can substantially affect climate due to their optical properties (Moise et al., 2015) and their ability to act as cloud condensation nuclei (CCN) (McFiggans et al., 2006), while their potential adverse effects on human health have recently drawn the attention (Chowdhury et al., 2018;Kramer et al., 2016).
45 Our current mechanistic understanding and the resulting SOA representation in predictive models remains inadequate (Shrivastava et al., 2017;McFiggans et al., 2019), leading to significant uncertainty of the assessment of their impacts.

The analytical limitations in the characterization and detection of all oxidation products as well as the complexity of the ever-evolving atmosphere (Isaacman-VanWertz et al., 2018), makes the understanding of the SOA behaviour
50 challenging. Atmospheric simulation chambers have been employed as a tool to study the formation and aging of SOA under simplified conditions (Burkholder et al., 2017). The oxidation of biogenic VOC (bVOC) and particularly terpenes has been studied extensively in chamber experiments, mainly as a result of their large contribution to global emissions (Spracklen et al., 2011) and their strong SOA formation potential (Lee et al., 2006). Although anthropogenic VOC (aVOC) emissions contribute less to the global emissions (Goldstein and Galbally,
55 2007) than the respective biogenic (Aiken et al., 2009), at a regional scale their relative emissions may be substantially higher, therefore they have been widely studied as SOA precursors in chamber experiments (Baltensperger et al., 2005;Wyche et al., 2009). These experiments have shown that both biogenic and

anthropogenic VOC oxidation can yield hundreds or thousands of products that are highly reactive and have wide range of volatilities (Hallquist et al., 2009).

60 A number of studies have shown that SOA volatility is largely dependent on the functionality through control of the vapour pressures (and to a lesser extent, the activity coefficients) of the individual organic compounds in the mixtures (McFiggans et al., 2010;Barley et al., 2009;Topping et al., 2011). Condensed phase reactions may further alter the SOA volatility (Kroll and Seinfeld, 2008). Therefore, the chemical reactions in both the gas and condensed phases determine the aerosol volatility, which in turn drives the partitioning of the species and the subsequent
65 transformation pathways.

Recently, the formation of highly oxygenated organic molecules (HOM), defined as organic compounds with at least 6 oxygen atoms through the autoxidation of peroxy radicals (RO_2) (Bianchi et al., 2019), has been shown to be a critical process affecting the growth of newly formed particles (Tröstl et al., 2016;Stolzenburg et al., 2018). The fate of RO_2, which can participate in autoxidation or other explicit termination reactions such as RO_2+HO_2,
70 RO_2+NO and RO_2 cross-reactions, has a determinant role for the HOM formation and volatility (Schervish and Donahue, 2020). HOM volatility is thought to range from the semi-volatile to the ultra-low volatility range.

Chamber studies have mainly focused on studying the formation and the resulting properties of the SOA formed from a single VOC precursor. Recently however, McFiggans et al. (2019) showed that upon mixing bVOC precursors, the SOA formation is governed by the molecular interactions of the products. Specifically, it was shown
75 that upon mixing a high and a low yield bVOC (α-pinene and isoprene, respectively), the overall SOA formation was suppressed due to i) the hydroxyl radical (OH) scavenging by the lower yield isoprene and ii) due to product scavenging. In the second process, the peroxy radical (RO_2) oxidation products of isoprene were scavenging the highly oxygenated RO_2 oxidation products (HOM-RO_2) of the higher yield precursor, leading to higher volatility products than if their termination partners had been other HOM-RO_2. This demonstrates that product interactions
80 in mixed precursor systems will alter the product distribution with consequent implications to the SOA formation and properties.

In this work, we extend the system studied by McFiggans et al. (2019) with the investigation of the interactions of an aVOC with a bVOC. We selected *ortho*-cresol (hereafter *o*-cresol), a product of toluene oxidation and also a directly emitted aromatic species, as a representative aVOC. In each system, the initial concentrations of the
85 reactants were adjusted to have equal reactivity towards OH at the beginning of each experiment such that the

mixtures were initially iso-reactive towards the dominant oxidant in the system. *o*-cresol is a convenient choice, enabling similar concentrations of VOC to be used in initially iso-reactive mixtures, owing to its relatively high reactivity with OH and moderate SOA yield (Atkinson, 2000;Henry et al., 2008). This choice of precursors and contributory reactivities enabled investigation of SOA formation with mixed systems containing a low, a moderate and a high yield precursor (i.e., isoprene, *o*-cresol and *α*-pinene, respectively) with equal initial chances of reacting with the dominant oxidant and contributions of first-generation oxidation products. This manuscript focuses on demonstrating the ability of the available tools to explore the SOA particle volatility using the *α*-pinene and *o*-cresol subset of the system as a proof of concept. Subsequent manuscripts will focus on the SOA formation dynamics and other aspects of the binary and ternary mixtures.

95 The SOA particle volatility in single precursor systems has been investigated based on the aerosol evaporation after heating (Lopez-Hilfiker et al., 2015;Donahue et al., 2006), by isothermal dilution (Yli-Juuti et al., 2017) or a combination of the two (Louvaris et al., 2017;Cain et al., 2020). Previous works have showed that the oxidation of *α*-pinene results in low volatility and semi-volatile components (Zhang et al., 2015). The oxidation of *o*-cresol has been studied to much lesser extent and the resulting SOA is thought to be composed of lower volatility species 100 compared to that derived from biogenic precursors (Baltensperger et al., 2005). Low and extremely low volatility material formed from oligomerisation reactions might contribute considerably to the *α*-pinene-derived SOA particle mass (Lopez-Hilfiker et al., 2015). Aromatic oxidation proceeds through rapid multiple generations of OH oxidation resulting in more oxygenated and less volatile material compared to biogenic precursors (Garmash et al., 2020;Wang et al., 2020).

105 In this study, we employ two independent thermal techniques (thermal denuder and FIGAERO coupled to a high resolution time of flight chemical ionisation mass spectrometer) and we aim to provide the first observational quantification of the volatility of SOA formed from an aVOC and bVOC precursor mixture with modest and high yields, respectively. Additionally, we use detailed gas and particle phase composition measurements to contextualise our volatility estimations and identify the main drivers of the SOA particle volatility in such mixtures. 110 We further aim to investigate the ability of the instrumentation used in exploring the SOA particle volatility and discuss their implications to the interpretation of the results.

2. Materials and methods

2.1. Manchester Aerosol Chamber

115 The experiments were conducted at the University of Manchester Aerosol Chamber (MAC) facility (Alfarra et al., 2012). MAC is an 18 m^3 fluorinated ethylene propylene (FEP) bag mounted on three rectangular frames, enclosed in a temperature and relative humidity (RH) controlled housing, operating as a batch reactor. The central frame is fixed whereas the lower and upper frames are free to move, allowing the bag to collapse and expand as chamber air volume changes, maintaining atmospheric pressure without dilution. Light is generated by a series of halogen

120 lamps (Solux 50 W/4700 K, Solux MR16, USA) and two 6 kW Xenon arc lamps (XBO 6000 W/HSLA OFR, Osram) over the range of 290-800 nm. Quartz glass filters were used in front of each arc lamp in order to reduce the radiation flux below 300 nm and mimic the atmospheric radiation spectrum as closely as possible. The photolysis rate of NO$_2$ (J_{NO2}), as computed from steady-state actinometry experiments, was 0.11-0.18 min^{-1}. The O$_3$ formed by NO$_2$ photolysis was itself photolysed in the moist chamber atmosphere (RH =~50%) to yield a OH

125 concentration from primary production, as calculated by the decay rate of solely OH reacting VOCs (e.g., toluene, o-cresol), of around 1×10^6 molecules cm^{-3}. Liquid VOC precursors (α-pinene and o-cresol; Sigma Aldrich, GC grade ≥99.99% purity) were added to the chamber by injecting the desired amount into a heated glass bulb and transferred into the chamber using gentle electronic capture device-grade nitrogen stream. Seed particles were nebulised using an aerosol generator (Topaz model ATM 230) from aqueous solutions of ammonium sulfate

130 (Puratonic, 99.999% purity). NO$_x$ concentration was controlled by adding the desired amount of NO$_2$ from a cylinder using ECD N$_2$ as carrier gas. All the reactants (VOC, NO$_x$ and seed) were introduced to the chamber at high flow rate (~3 m^3 min^{-1}) during the final fill cycle, resulting in rapid mixing. The mixing and temperature control throughout the experiment was effected through the use of conditioned air circulated at high flowrate around the chamber housing, continually agitating the chamber walls without physical contact.

135

2.2. Experimental procedure

The experiments conducted in this study were representative of "daytime" photo-oxidation in the presence of O$_3$ and OH. This study, as also described above, is part of a broader project investigating SOA derived from mixtures of precursors with distinct yields and properties. Here, we focus on the α-pinene and o-cresol system, as

140 representative biogenic and anthropogenic VOC precursor sources (Hallquist et al., 2009;Schwantes et al., 2017),

both with appreciable SOA yields (e.g., Henry et al., 2008;Kristensen et al., 2014). In order to study the effect of mixing anthropogenic and biogenic precursors on SOA particle volatility, two types of experiments were conducted: (a) single precursor experiments, where the photo-oxidation of each precursor was studied individually and (b) mixture experiments, where both precursors were added to the chamber simultaneously. Since o-cresol is

145   practically unreactive towards O_3 within our experimental timescales and because α-pinene's lifetime with respect to OH is shorter than towards O_3 at the expected oxidant concentrations in our experiment (5.2 vs 6.3 h; Atkinson, 2000), the concentrations of the reactants were selected based on the reactivity of each precursor with OH. As such, each VOC has equal initial chances of reacting with the dominant oxidant in the mixture experiments, while the overall initial reactivity (defined as the product of the VOC concentration and the reaction rate coefficient with

150   OH) in both single-precursor and mixture experiments was the same. Therefore, our systems are "iso-reactive" at the beginning of each experiment, though not necessarily thereafter. The ozone concentration at the beginning of each experiment was zero. Ozone is formed rapidly from the photolysis of NO_2 after the lights are turned on to establish photostationary state and then continuously produced through the oxidation of VOC in the presence of NO_x (Atkinson, 2000). All the experiments were conducted under modest NO_x conditions (VOC/NO_x 6±2 ppb/ppb)

155   by adding NO_2, and moderate RH and temperature conditions (50±5% and 24±2 ℃, respectively). Ammonium sulfate seed particles (53±12 μg m^{-3}) were added to provide a medium for condensation of the condensable VOC oxidation products to successfully compete with the walls, to reduce the influence of vapour wall-losses and also to suppress nucleation (Zhang et al., 2014). The initial experimental conditions are summarised in Table 1.

Each experiment was comprised of a common set of procedures shown in Fig. S1a. Briefly:

160   i)   The "pre-experiment" procedure entailed flushing of the chamber with clean air at a high flow rate of 3 m^3 min^{-1} for ~1.5 h.

ii)   The "chamber background" was established by stabilising the chamber with clean air without reactants. This phase lasted for ~1 h and the established baselines were thereafter subtracted from the measurements.

165   iii)   The "dark unreactive" phase commenced after the addition of the VOC precursor(s), NO_2 and seed aerosol to the chamber in the dark. During this period (also ~ 1 h), the initial conditions of the chamber were established.

iv)   The "experiment" phase commenced when the chamber lights were turned on, initiating the photo-oxidation and consequent SOA formation. Each "experiment" phase lasted for 6 h.

170   v)   A "post-experiment" cleaning procedure normally comprised the high flowrate flushing of the chamber with clean air for ~1.5 h, subsequently filling with high concentration of O_3 (≥1 ppm) and soaking overnight to oxidise any remaining gas-phase organic species. All the results given below correspond to the "experiment" phase only.

175   **Table 1: Summary of the initial conditions for each of the experiments conducted in this study.**

Experiment No.	Experiment type	NO_x (ppb)	VOC (ppb)	VOC/NO_x (ppb/ppb)	Seed Concentration (µg m⁻³)
	Single VOC				
1	α-pinene	40	309	7.7	72.6
2	α-pinene	43	309	7.2	67.6
3	α-pinene	37	309	8.4	62.0
4	α-pinene	50	309	6.2	39.4
6	o-cresol	71	400	5.6	36.0
7	o-cresol	44	400	9.1	47.8
8	o-cresol	56	400	5.0	51.3
	Mixture				
9	α-pinene+o-cresol	n.a.[*]	355 (155+200)[a]	n.a.[*]	42.5
10	α-pinene+o-cresol	30	355 (155+200)[a]	11.8	57.0
11	α-pinene+o-cresol	52	355 (155+200)[a]	6.8	48.3

[*]**n.a. values correspond to corresponding instrument failures at the day of the experiment.**

[a]**Sum of the VOC added in the mixture the individual concentrations of α-pinene and o-cresol added are shown in the brackets, respectively.**

2.3. Instrumentation

2.3.1. TD- AMS/SMPS

A scanning mobility particle sizer (SMPS; DMA 3081 and CPC 3776, TSI Inc., USA) was used to measure aerosol size distributions in the range of 10-670 nm, operating at 0.3 L min^{-1} (1:10 sample/sheath flow). The non-refractory aerosol chemical composition and mass were measured by a high-resolution time of flight aerosol mass spectrometer (HR-ToF-AMS, ARI Inc., USA hereafter HR-AMS) (DeCarlo et al., 2006), sampling at 0.1 L min^{-1}. The HR-AMS was calibrated regularly using previously published procedures (Jimenez et al., 2003;Allan et al., 2004).

The TD unit employed here was designed based on the recommendations of Fuentes and McFiggans (2012). Briefly, sample flow enters and exits the TD unit via a cylindrical 0.12 m long and 36.6 mm inner diameter (ID) stainless steel compartment. The heating section which is placed in a housing with insulating material, has a length of 0.51 m and an ID of 151 mm, and its temperature is controlled by four PID controllers (Watlow EZ-ZONE). A cooling section with a length of 0.2 m and an ID of 20 mm, allows the sample to cool down to ambient temperature with minimal re-condensation (Fuentes and McFiggans, 2012). In our configuration, the TD was operating at temperatures ranging from 25 to 90 °C in 13 steps and the HR-AMS and SMPS sampling alternated between the bypass and TD every 4 and 6 min, respectively, using a 3-way electronic valve. The alternating sampling through the TD unit was initialised at the final 2 h of each experiment where minimal changes in the aerosol composition over time are expected (i.e., SOA formation rate<wall loss rate). The resulting mass fraction remaining (MFR) in each temperature step was calculated as the ratio of the total aerosol mass passing through the TD to the average bypass concentration obtained before and after each step. The sample flow rate through the TD and bypass was adjusted to 1 L min^{-1}, resulting in an average residence time of the aerosol in the heating section of 31 s, using a vacuum line and a mass flow controller. All the TD data were corrected for particle losses as a function of particle size and temperature, based on characterisation experiments conducted using sodium chloride particles and the same instrument configuration.

2.3.2. FIGAERO-ToF-CIMS

Near-real time gas and particle composition was measured using the Filter Inlet for Gas and Aerosols (FIGAERO) (Lopez-Hilfiker et al., 2014) coupled to an Iodine high-resolution time of flight chemical ionisation mass spectrometer (Lee et al., 2014) (hereafter FIGAERO-CIMS). Briefly, the FIGAERO manifold allows the

determination of both particle and gas phases by collecting particles on membrane filter while sampling the gas phase. After a period of time, the deposited aerosol is thermally desorbed using high purity N_2 as a carrier gas. In

210 our setting, particles were sampled from the middle of the chamber through a 2 m long, 0.635 cm OD stainless steel tube at 1 sL min^{-1} and deposited on a PTFE filter (Zefluor, 2.0 µm pore size). The flow over the filter is continually monitored by an MKS mass flow meter (MFM) after the sample has passed over the filter so ensure a known volume is sampled in each cycle. The gas phase was sampled through a separate line, using a 2 m long, 0.635 cm OD PTFE tubing, in order to minimise any potential gases losses into the lines (Sulyok et al., 2002;Mittal

215 et al., 2013), at 2 sL min^{-1}. This gas phase sample flow is again constantly measured a MFM at the exhaust of the IMR pump which included the reagent ion flows. The instrument was run in negative-ion mode with I$^-$ reagent ion in all the experiments. The reagent ions were produced by passing a known concentration mix of CH_3I and UHP N_2 over a PO_{210} radioactive source and passed directly into the IMR.

The FIGAERO-CIMS was configured in operating in cyclic mode with 30 min of gas sampling and simultaneous

220 particle collection, followed by 15 min of thermal desorption from ambient to 200 °C (~12 °C min^{-1}; temperature ramp period) and then kept at a constant temperature for another 10 min (i.e., soak period) to ensure that all the remaining mass is evaporated. Last, the FIGAERO was cooled down to ambient temperature within 10 min (i.e., cooling period). An example of the FIGAERO cycle is shown in Fig. S1b. Further details on the FIGAERO-CIMS employed in this study can be found in Bannan et al. (2019) and Priestley et al. (2018). In order to account for any

225 potential instrument contamination during the gas-phase sampling, the instrument was flushed with UHP N_2 for a period of 0.2 min every 2 min, thus a gas phase instrument background value was regularly established and applied to the final data by linear interpolation (Fig. S1b).

As a result of the low organic particles concentration in the first hours of the *o*-cresol experiment and for comparison with the concurrent TD measurements, all the results shown by the FIGAERO-CIMS here correspond to the data

230 obtained during the last two hours of the experiment.

It should be noted that quantification from the FIGAERO-CIMS in both the particle and gas phase remains challenging as a result of a lack of available standards and the experimental limitations (Riva et al., 2019). Despite a number of studies attempting to constrain those limitations (Lopez-Hilfiker et al., 2016a;Aljawhary et al., 2013), this remains extremely challenging. Therefore, here, we assumed uniform instrument sensitivity across the whole

235 range of the detected products and an assessment of the impact of increased sensitivity to particular functional group additions on the reported results is probed in Section 4.2.

2.4. Data analysis

2.4.1. FIGAERO-ToF-CIMS

240 The FIGAERO-CIMS data were analysed using the Tofware package in Igor Pro (v. 3.2.1., Wavemetrics$^©$) (Stark et al., 2015). The peak fitting was conducted in the region of 190-550 m/z, where the vast majority of the total signal occurred (>70%; excluding the reagent ions; I^- I_2^- I_3^- and $I.H_2O^-$). The mass to charge calibration was performed in the range of 127-380 m/z using four known masses, I^-, $CH_2O_2I^-$, I_2^- and I_3^- and the resulted calibration error was within 3 ppm. The remaining ions were sorted based on their contribution to the total signal and the HR

245 formula identification was conducted until more than 80% of the total fitted signal was assigned. All the elemental formulae were assigned to the HR spectrum according to Kendrick's mass defect, all within ~6 ppm error. Only the particle phase data collected during the temperature ramp were considered here due to signal interferences observed during the soak period. These interferences could be attributed to the prolonged period of flushing the instrument with high temperature gas and/or burning off inorganic/involatile material from the filter (Wang and

250 Hildebrandt Ruiz, 2018). The gas-phase data obtained during "instrument background" mode (see Section 2.3 and Fig. S1b) were subtracted from the measured values in each cycle by linear interpolation. To account for any potential chamber contamination, the data obtained during the "chamber background" phase were also subtracted from the data obtained during the "experiment" phase (see Section 2.2 and Fig. S1b). For the particle-phase data, a similar procedure was followed. In certain cases, a high initial particle phase signal was observed that

255 subsequently decreased over time (Fig. S2a). To correct for these interferences a corresponding particle-phase "instrument background" period was assumed. We selected the 30-60th second of each desorption cycle as a particle-phase "instrument background" period (Fig. S1b) because (i) the desorption temperature was still at ambient levels (<22ºC; Fig. S2b), implying that the thermal desorption process had not yet started and (ii) this period avoided the "noisy" signal that appeared during the first 10-15 s of each desorption cycle produced by the

260 IMR pressure change due to the actuator shifting position (Fig. S2a). The average signal of the particle-phase "instrument background" period was then subtracted from the raw desorption data and the resultant thermograms (signal vs. desorption temperature) were integrated using the trapezoid rule. Subsequently, the integrated area of each peak obtained during the "dark unreactive" phase (see Section 2.2; Fig. S1a) was subtracted from the data to remove any seed and/or filter effect. All the subsequent analysis presented in this work is using the background-

265 corrected data.

In order to identify the products that are uniquely formed in the mixed VOC systems, we computed the signal contribution of each of the unique precursor products, as identified in the single VOC experiments, to the total signal of the FIGAERO-CIMS of the mixture in each phase. The contributions of products with assigned formulae which were common among all systems and CIMS is unable to resolve (i.e., isomers) were also computed, while the remaining were considered as unique to the mixture products. In order to take into account any potential products which were not identified in single experiments but still uniquely correspond to either of the two precursors and were potentially miscounted as unique to the mixture products, we compared the resultant products categorised as unique to the mixture with the Master Chemical Mechanism (MCM v3.2;Saunders et al., 2003;Jenkin et al., 2003). The unique to the mixture products that were matched with the products of either precursor from the MCM or were found as common, were subsequently assigned to the corresponding lists.

2.4.2. Volatility retrieval from TD-AMS

The Mass Fraction Remaining (MFR) data obtained from the SMPS/AMS were used to calculate the volatility distributions of the bulk SOA. The volatility distributions here were expressed as effective saturation concentration at 298 K (C^*; µg m^{-3}) bins in the Volatility Basis Set (VBS) framework (Donahue et al., 2006) and were calculated by the algorithm of Karnezi et al. (2014). Briefly, the approach uses the thermodynamic mass transfer model of Riipinen et al. (2010) to fit the MFR measurements of the thermodenuder selecting appropriate volatility distributions and effective enthalpies of vaporization. The model neglects any temperature gradients in the TD and assumes monodisperse aerosol population, equal to the mean volumetric diameter. The inputs of the model, in addition to the MFR measurements, were the average residence time in the heating section (31 s), the length of the heating section (0.51 m), the average volumetric diameter of the particles entering the TD (calculated from SMPS data for the by-pass line), the average organic mass concentration bypassing the TD and the particles' density (assumed as 1.4 g cm^{-3}). The volatility distribution was expressed in six volatility bins spanning from $C^*=10^{-3}$ to 10^2 µg m^{-3}.

3. Results

3.1. Gas and particle phase composition

Figure 1 shows the average ($\pm 1 \sigma$) distribution of carbon number of all the products identified by the FIGAERO-CIMS in each phase and system investigated. The distributions in the mixed VOC system show the contributions

from the products of either precursor, the common products and the products unique to the mixture, in addition to the unidentified fraction (see Section 2.4).

295 Each individual precursor system exhibited distinct features. For example, in the α-pinene single precursor system, the majority of the products identified by the FIGAERO-CIMS both in the gas and particle phase had the same or fewer carbon atoms than the parent molecule (81 and 73% of the total signal in each phase, respectively; Fig. 1). More specifically, in the particle phase, the highest contribution was found for products with 10 carbon atoms while in the gas phase for products with 7 carbon atoms. In contrast, in the o-cresol single precursor system, the vast

300 majority of the identified products in either phase showed a narrow distribution centred around the carbon number of the precursor (ie., nC=7). This can be associated with the large signal contribution of two individual products in each phase, assigned as $C_7H_8O_2$ (50%) and $C_7H_7NO_4$ (40%) in the gas and particle phase, respectively. In the particle phase of both single precursor systems, a greater fraction of the signal is associated with products having more carbon atoms than each precursor, compared to the respective gas phase contributions.

305 In both gas and particle phases in the mixed VOC system, the largest fraction of the total signal was found for products with 7 carbon atoms. In the gas phase, the remaining signal was distributed in the region of nC=4-10 with stronger contributions at nC=5 and nC=10, while in the particle phase, products with nC=8 and nC=10 contributed considerably to the total signal. Unlike the single precursor systems, the contributions of products with larger than 10 carbon atoms are not substantially different between the gas and particle phases.

310 The majority of the products that were common between all systems have low carbon numbers (nC<5) and account for a higher fraction of the total gas than the particle phase signal of the mixed VOC system (18% vs. 8%). In both phases, o-cresol products appear to contribute most to the total signal of the mixed VOC system with the majority of the signal in products with 7 carbon atoms, similar to the single precursor system. The products that were classified as unique products of the mixture account for approximately the same fraction in both phases and were

315 found mostly in the nC=5-10 range, with appreciable fractions in the nC>10 range.
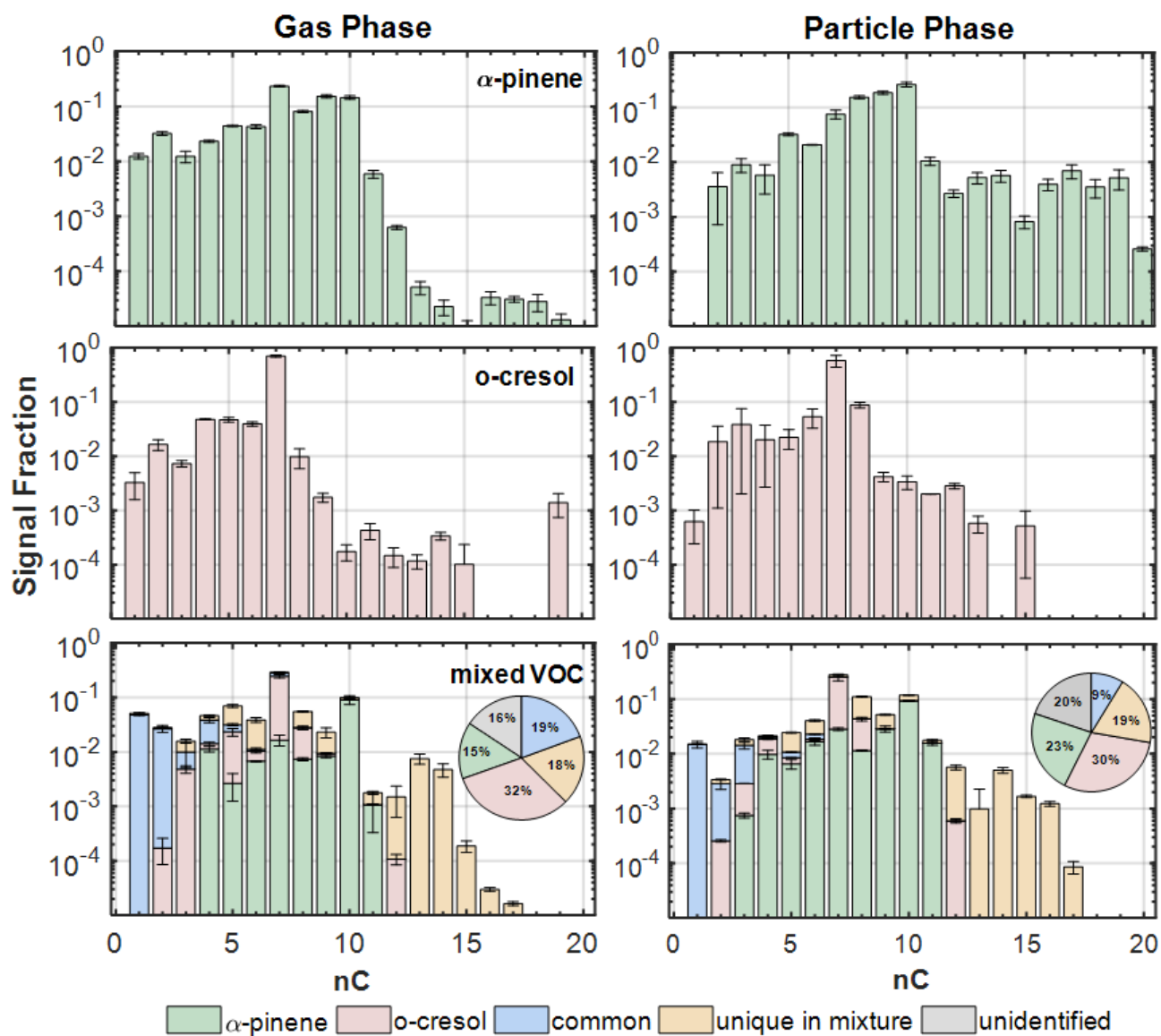
Figure 1: Average (± 1σ) distributions of carbon number (nC) of all individual products identified in the three systems for the gas (left panels) and the particle phase (right panels). In the mixed VOC system, the bars are separated to show the contributions of products that were associated with either precursor, the common ions as well as those that were found unique in the mixture. The above are summarised in inset pie charts to show to overall contributions to the total signal in each phase.

320

The O:C ratios in the particle phase show the contributions to SOA mass per condensed carbon attributable to O. The average (± 1σ) of O:C ratio for all the products identified in each system from the FIGAERO-CIMS, weighted

325 to the contribution of each product to the total signal along with O:C ratio derived from the HR-AMS are shown in the Figure 2. Both HR-AMS and FIGAERO-CIMS showed comparable results, with the O:C being highest in the *o*-cresol system (0.68 vs 0.56, respectively), followed by the mixed VOC (0.47 vs 0.49, respectively) and the *α*-pinene system (0.35 vs 0.45, respectively). Although N:C ratios might provide similarly useful information, their quantification with FIGAERO-CIMS and HR-AMS has been proven challenging as a result of sensitivity effects

330 (Iyer et al., 2016) and the extensive fragmentation which is not readily characterised for the N-containing fragments (Farmer et al., 2010), respectively.
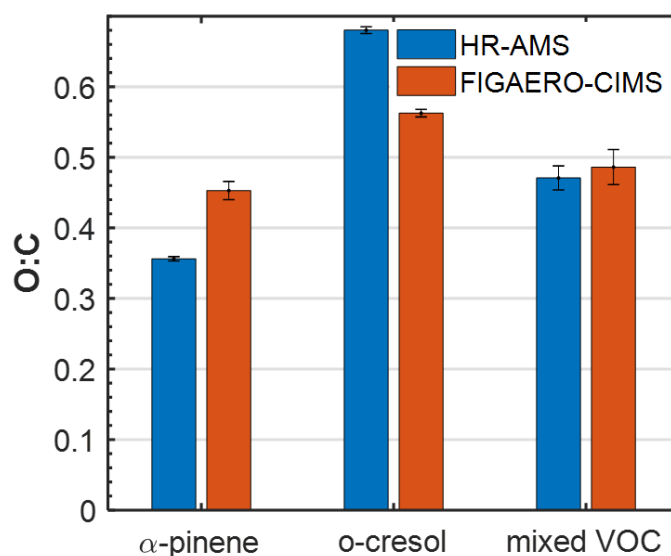
Figure 2: Average (± 1σ) oxygen to carbon (O:C) ratio for all the products identified in the particle phase from the FIGAERO-CIMS and the HR-AMS for each system.

335

3.2. SOA particle volatility

Our experimental setup allows the estimation of the SOA particle volatility distribution using two independent techniques. The TD measurements with the approach of Karnezi et al. (2014) allow the retrieval of the SOA particle volatility distribution in the VBS framework. For comparison, the thermal desorption of the SOA particles collected

340 on the FIGAERO provides an indirect measure of the volatility as a function of the FIGERO-CIMS total particle

phase signal (Lopez-Hilfiker et al., 2014;Lopez-Hilfiker et al., 2016b).

3.2.1. Insights on the SOA particle volatility from the FIGAERO-CIMS

Figure 3, shows the average sum thermograms for each system (± 2σ as shaded areas). For the mixture, the

contributions from the products of either precursor, the common products, the unique to the mixture products in

345 addition to the unidentified fraction are shown in Figure 1b as areas for a characteristic experiment (Exp. no. 10;

Table 1). Furthermore, here, we define the products evaporating at ≤50ºC as "more volatile", those evaporating

between 50 and 90ºC as "moderately volatile" and those evaporating above 90ºC to be "less volatile" (e.g., Saha

and Grieshop, 2016;D'Ambro et al., 2019;Lopez-Hilfiker et al., 2014). Figure 4 shows the corresponding signal

fraction that evaporated in each of these desorption temperature bins in three characteristic experiments (Exp. No.

350 2, 5 and 10; Table 1). The sum thermogram in the α-pinene system is broader compared to the other systems and

peaked at relatively low temperature (60 ºC). Characteristically, the fraction of the signal evaporated at the ≤50,

50-90 and ≥90 ºC range was 11, 27 and 62%, respectively. In contrast, the sum thermogram in the o-cresol

experiment was narrower, peaking at 80 ºC, while the corresponding fractions evaporated were 4, 35 and 61%. The

sum thermogram in the mixed VOC system peaked in the mid-temperature range (70 ºC), while its distribution

355 appeared to have similar features as those from the single precursor experiments. More specifically, the sum

thermogram of the mixture exhibited similar fraction of products desorbing at lower temperatures as the o-cresol

experiment (4% of the total signal desorbed at ≤50 ºC) and similar fraction of products desorbing at higher

temperatures as those in the α-pinene experiment (64% of the total signal desorbed at ≥90 ºC). This suggests that

the SOA particles from α-pinene photo-oxidation have higher contributions of both higher and lower volatility

360 material, those from o-cresol oxidation have narrower volatility distribution and modest volatilities, and those

formed from the photo-oxidation of the mixture of both precursors to be moderate to less volatile.
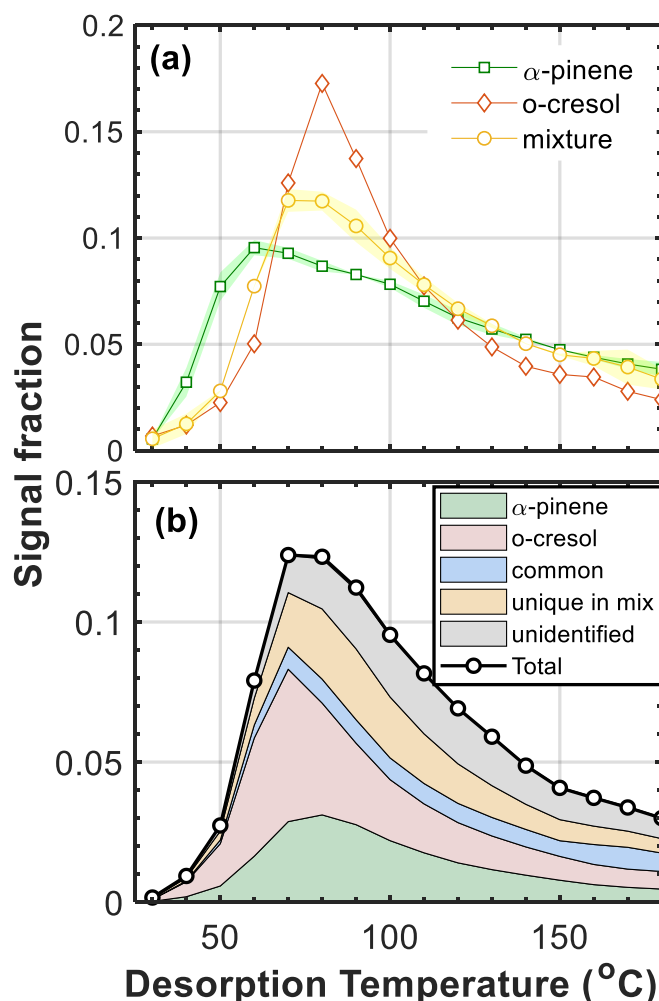
Figure 3: (a) FIGAERO-CIMS average (± 2σ as shaded areas) sum thermograms in each system and **(b)** Example sum thermogram from a mixed VOC experiment (Exp. No. 10; Table 1) where the contributions of products that were associated with either precursor, the common products, those that were found unique in the mixture, in addition the unidentified fractions are shown as areas.

The products from the *o*-cresol oxidation contribute substantially to the total signal in the 50-90 ºC and ≥90 ºC range of the mixed VOC experiment (12 and 10%, respectively), whereas those deriving from the oxidation of *α*-pinene contribute most to the ≥90 ºC range and to a lesser extent to 50-90 ºC range (12% and 8%, respectively). The common products mostly contribute to the ≥90 ºC range (7%), with smaller contributions to the 50-90 ºC bin

(2%). The products that were unique to the mixture contribute mostly to the ≥90 ºC range (12%) and considerably to the 50-90 ºC range (6%). Notably, the unidentified ions were contributing 21% of the signal in the ≥90 ºC range. This shows that the products from either precursor as well as those that were common in both systems have

375   moderate to low volatilities, while those that were classified as unique products of the mixture mostly have lower volatilities.

It should be noted however that the high contribution from the *o*-cresol products in the mixture at the 50-90 ºC range, as well as the narrow desorption temperature distribution observed in the single *o*-cresol system, was significantly influenced by the dominant product (i.e., $C_7H_7NO_4$). The implications of this in the interpretation of

380   the results will be further discussed in Section 4.2.
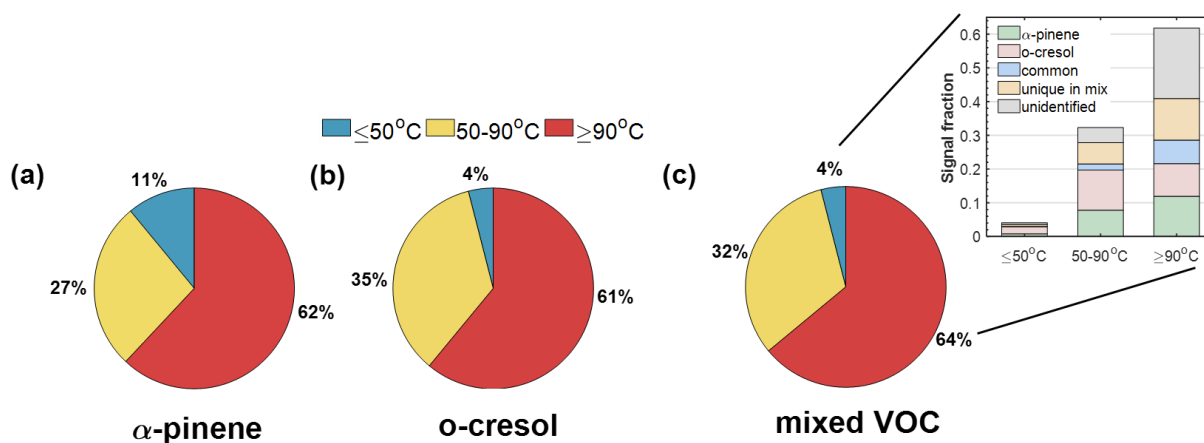
Figure 4: FIGAERO-CIMS signal fraction that evaporated at ≤50, 50-90 and ≥90 ºC in a characteristic (a) *α*-pinene, (b) *o*-cresol and (c) mixed VOC experiments (Exp. No. 2, 5 and 10, respectively). For the mixed VOC experiment, the inset bar chart shows the contributions of the products of each precursor, the common

385   **and the unique to the mix products as well as the unidentified fraction.**

3.2.2.   Insights on the SOA particle volatility from the TD-AMS

The predicted SOA particle volatility distributions from the TD measurements for the same characteristic experiments (Exp. No. 2, 5 and 10; Table 1) are presented in Figure 5, expressed in effective saturation

390   concentration at 298 K (C^*) bins in the VBS framework. The bin with $C^*=10^{-3}$ µg m^{-3} includes also the less volatile material (extremely low volatility organic compounds) and the bin with $C^*=10^2$ µg m^{-3} may also include more

volatile material. The material with $C^* \geq 1$ µg m^{-3} is characterized as semi-volatile organic compounds (SVOCs) while that with $C^* \leq 0.1$ µg m^{-3} has low volatility (LVOCs). The volatility distribution of the SOA formed in the α-pinene experiment, indicates a higher contribution of species with $C^* \geq 100$ µg m^{-3}, compared to o-cresol and

395   mixture experiments. Conversely, in the o-cresol and in the mixture experiments the bins with $C^* \leq 0.1$ µg m^{-3} exhibited relatively higher values compared to the single precursor α-pinene system, suggesting a higher contribution of less volatile material. More specifically, the mass fraction of the LVOC and SVOC was 28 and 72% for the α-pinene SOA, 39 and 61% for the o-cresol SOA and 37 and 63% for their mixture, respectively.
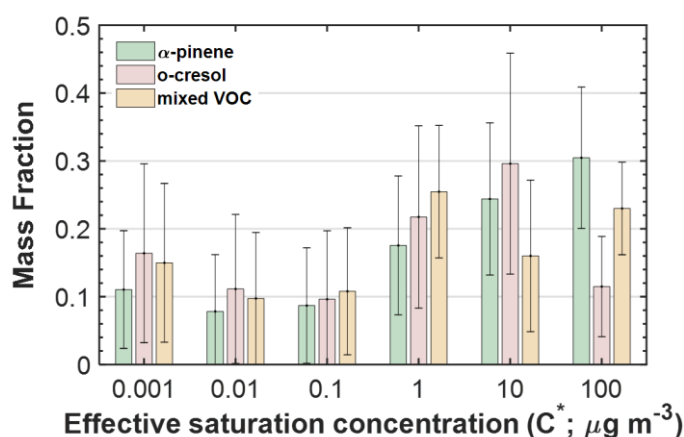
400   **Figure 5: SOA particle volatility distributions retrieved from the TD measurements for three characteristic experiments (Exp. No. 2, 5 and 10; Table 1).**

The volatility distribution inversion algorithm employed here (Karnezi et al., 2014) can also provide the enthalpy of vaporisation and the mass accommodation coefficient for each of the experiments investigated. The enthalpy of

405   vaporisation was found to be higher in the α-pinene experiment (120 kJ mol^{-1}) and lower at the o-cresol (106 kJ mol^{-1}). This qualitatively consistent with the larger size of the molecules in the α-pinene SOA. The mass accommodation coefficients were close to unity in both systems (0.36 for the α-pinene and 0.23 for the o-cresol SOA; Fig. S3) suggesting only small resistances to mass transfer in the temperature range of the TD. The respective values for the mixed VOC experiment were found to be intermediate of those for the individual single-precursor

410   systems (109 kJ mol^{-1} and 0.27, respectively). Nonetheless, due to the corresponding uncertainties which were ± 20% for the enthalpy of vaporisation and much higher for the mass accommodation coefficient, these differences may not reflect the reality.

The relationship between the O:C and the MFR can provide indirect additional information about the volatility of the species in each system. Figure 6 shows the O:C enchantment ratio (i.e., O:C at the TD line divided by the corresponding O:C at the BP line) as a function of the particle MFR for a number of experiments in each system. The increasing O:C enhancement ratio as the MFR decreases in all systems is indicating that as the temperature in the TD increases, the remaining SOA particles are less volatile and more oxygenated, consistent with previous observations in chamber experiments (e.g., Huffman et al., 2009). All systems appeared to behave similarly at low TD temperatures (<40 ºC), with the O:C enhancement ratio being between 1 and 1.04 and MFR>80%, implying the existence of products with similar degree of oxygenation and similarly high volatility. However, at higher TD temperatures (>40 ºC), each system showed distinctive features. The SOA particles from the *o*-cresol system showed the highest O:C enhancement ratio, reaching up to 1.16, followed by those from the mixed VOC and the *α*-pinene system which exhibited similar maximum values (1.097 and 1.091, respectively). More specifically, the slope between the highest O:C enhancement ratio and the MFR was twice as high in the *o*-cresol compared to *α*-pinene systems, whereas that of the mixed system was approximately between. These results indicate that the less volatile SOA particles from the *o*-cresol system are considerably more oxygenated compared to the average than those of the *α*-pinene system.
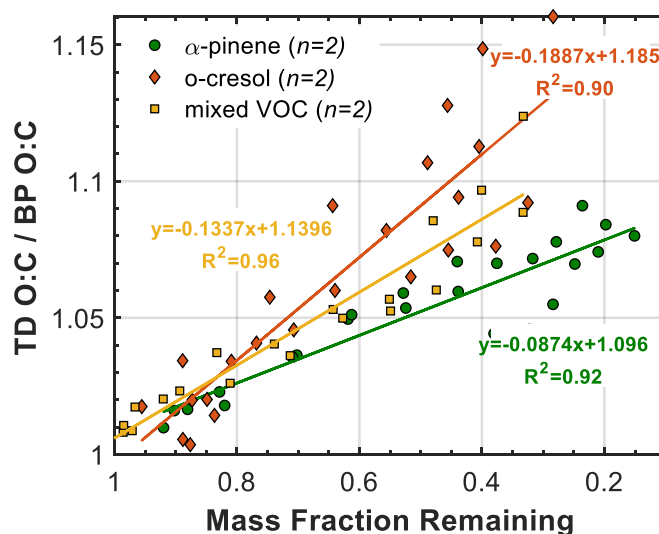
Figure 6: O:C enchantment ratio (i.e., O:C at the TD line divided by the corresponding O:C at the BP line) as a function of the particle MFR in each system investigated.

3.2.3. Comparison of the SOA particle volatility between FIGAERO-CIMS and TD-AMS

The FIGAERO-CIMS is able to detect a subset of the total SOA (Lee et al., 2014;Lopez-Hilfiker et al., 2014), whilst the TD technique is able to derive bulk estimations. The increased material in the $C^*\leq0.1$ μg m^{-3} bins in the
435   o-cresol and mixed VOC systems compared to that of $α$-pinene are consistent with the increased number of products having relatively higher maximum desorption temperatures. Similarly, the increased $C^*=100$ μg m^{-3} content observed in the $α$-pinene system compared to the other systems is consistent with the increased fraction of its products desorbing at relatively lower temperatures (i.e., ≤ 50ºC; Fig. 4). The SOA volatility distribution of the mixed VOC system appeared to be between those of o-cresol and $α$-pinene (Fig. 5), which is also consistent with
440   the sum thermograms of its products (Fig. 3). This broad consistency between the volatility inferred from TD inversion and FIGAERO-CIMS provides some confidence that the analysis presented here may be representative of the bulk SOA particle composition.

4.   Discussion

445

4.1.   Linking the gas and particle chemical composition to SOA volatility

The gas and particle phase composition, as can be obtained by the FIGAERO-CIMS, can provide indications about the systems chemical behaviour and thereby the potential effect on SOA volatility. Oligomerisation is a process that increases the products' molar mass decreasing their volatility while tending to maintain their O:C.
450   Functionalisation also decreases a compound's volatility by the addition of oxygenated functional groups and thus increasing their O:C ratio. Fragmentation (i.e., cleavage of carbon-carbon bond) will increase component volatility due to the decrease of the product's molar mass, though in some cases the fragmented products are subsequently functionalised (e.g., O$_2$ addition after the scission of a double bond) leading to a decrease of their vapour pressure, with the net effect on vapour pressure not immediately predictable.

455   The FIGAERO-CIMS results described above indicate that fragmentation is a major process occurring in all the systems due to the significant fraction of products having lower carbon numbers than their precursors (Fig. 1). Of course, it should be noted that the interpretation of FIGAERO data is dependent on the components that are readily accessible using the chemical ionisation scheme. The iodide CIMS (I$^-$-CIMS) has a wider range of sensitivity than acetate or NO$_3^-$ instruments although each detects a subset of those components that are present at varying
460   sensitivity (Riva et al., 2019). The I$^-$-CIMS is efficiently detecting compounds in the IVOC and SVOC range with

modest carbon and oxygen numbers while NO_3^--CIMS is more sensitive towards compounds in the LVOC and ELVOC range with higher carbon and oxygen numbers, such as HOM (Priestley et al., 2021). This suggests that the observed relatively lower contributions of higher molecular weight compounds might be related to the sensitivity of the technique employed here. Nonetheless, considering that previous studies have showed that the

465 contribution of HOM to the SOA mass is minor (Rissanen et al., 2014;Jokinen et al., 2014), and the general agreement between the FIGAERO-CIMS and the TD-AMS might indicate that the I^--CIMS might be able to capture the bulk SOA composition.

Given the above, the effect of fragmentation is more pronounced in the α-pinene system, in agreement with previous findings (Eddingsaas et al., 2012b;Eddingsaas et al., 2012a) potentially explaining the higher fraction of more

470 volatile products with $C^* \geq 100$ μg m^{-3} compared to the other systems (Fig. 5). This is also consistent with the increased fraction of products desorbing at relatively lower temperatures (Fig. 4). On the other hand, the increased number of products in the nC>10 region compared to the other systems, shows that gaseous and/or condensed phase oligomerization/dimerisation reactions are also taking place during the a-pinene SOA formation (Lopez-Hilfiker et al., 2015). Their relatively low contribution to the total FIGAERO-CIMS signal might indicate that they

475 will make little contribution to the mass of the $C^* \leq 1$ μg m^{-3} volatility bin considering that the α-pinene SOA mass is lower in these bins than in other systems(Fig. 5). These dimers probably are not responsible for the majority of the LVOCs in the SOA formed in the corresponding experiments.

In o-cresol experiments, the OH addition via hydrogen abstraction pathway which mainly leads to low volatility ring-retaining products (Olariu et al., 2002;Schwantes et al., 2017), contributes substantially to the total FIGAERO-

480 CIMS signal, considering that the largest fraction of its signal is found for products with 7 or more carbon numbers (Fig. 1). Additionally, the elevated O:C in the o-cresol system and its stronger O:C enhancement ratio compared to the other systems (Fig. 2 and Fig. 6) is consistent with its overall low volatility (Fig. 4). The oxygen addition pathway, leading to bicyclic intermediates that subsequently decompose to smaller multifunctional compounds (Schwantes et al., 2017), may be also responsible for the presence of the smaller molecules. This latter pathway

485 can have complex effects in both directions for the resultant SOA volatility.

The SOA formed in the mixed system may comprise i) products of either precursor, ii) cross-products formed in the particle or gas phase (with sufficiently low volatility to partition to the particle phase) and iii) individual precursor products resulting from the alteration of the oxidation mechanism of each precursor due to the interactions. It should be noted that our formula separation technique is unable to identify any new individual

490   precursor products from (iii) that are not listed in the MCM (see 2.4.) and would classify them as products unique

to the mixture. Products unique to the mixture with nC=5-10 represent the largest fraction of the corresponding

total signal (Fig. S2). The formation of these products, as well as those with nC>10, could be both attributed to

processes described above for each individual VOC and/or interactions between the resultant products (such as

RO$_2$+R'O$_2$ termination reactions, with R and R' from o-cresol and α-pinene respectively). The volatility of these

495   products, as inferred from their maximum desorption temperatures, is on average, lower than that of the respective

products of the bulk with the same carbon numbers (i.e., individual precursor's plus common products in the

mixture; Fig. 7). This decrease in volatility of the products unique to the mixture may be partly attributed to

increased O:C content of those products compared to those of the bulk (Fig. S4). This suggests that the mixing of

α-pinene and o-cresol results in unique products that are more oxygenated than the respective products of the bulk,

500   and consequently have lower volatilities.

The unique products to the mixture that have lower carbon numbers (nC<5) were likely formed from small organic

radical termination reactions deriving from each individual precursor and/or from the fragmentation/dissociation

of larger cross- products and/or from the thermal decomposition of products in the FIGAERO (Stark et al., 2017).

The vast majority of those products were found to be common between all experiments and contribute a higher

505   fraction of the signal in the gas compared to the particle phase, making thermal decomposition unlikely to be the

source of the largest fraction of these products. These products exhibit high O:C, consistent with their high

desorption temperature and lower volatility (Fig. 7 and Fig. S4). Comparing their characteristics to the respective

products of the bulk, similar conclusions can be drawn as for the corresponding larger products (nC≥5), i.e., the

unique to the mix products with nC<5 appear to have higher O:C and desorption temperatures than those of the

510   bulk. It should be noted that these products contribute minimally to the total signal of the particle phase (Fig. 1),

thereby their effect of the overall SOA volatility is expected to be correspondingly low. Nonetheless, this

demonstrates that the unique to the mix products are, on average, less volatile than the individual products of both

precursors and those that were common that are found in the mixed VOC system, across the whole range of carbon

numbers.

515   The retrieved SOA particle volatility from the mixed VOC system showed an increased content of lower volatility

components compared to the α-pinene system while being comparable with that from the o-cresol system. The

compositional information obtained suggest significant signal contributions from the unique products of o-cresol

in the mixed system, which are of lower volatility compared to α-pinene's (Figs. 4-6). Furthermore, it is apparent

that the higher carbon number products that were formed in the α-pinene system and are expected to have lower

520   volatilities (Kroll and Seinfeld, 2008), are absent in the mixed VOC experiment (Fig. 1), suggesting that molecular

interactions can also increase the volatility in mixtures (McFiggans et al., 2019). Meanwhile, the products that were

only formed in the mixture are also contributing considerably to the total signal and are lowering the overall

volatility (Fig. 7). This shows that upon mixing SOA precursors, the underlying molecular interactions can increase

or decrease the SOA particle volatility in mixtures and the resultant particle volatility in mixed systems cannot be

525   readily deduced.
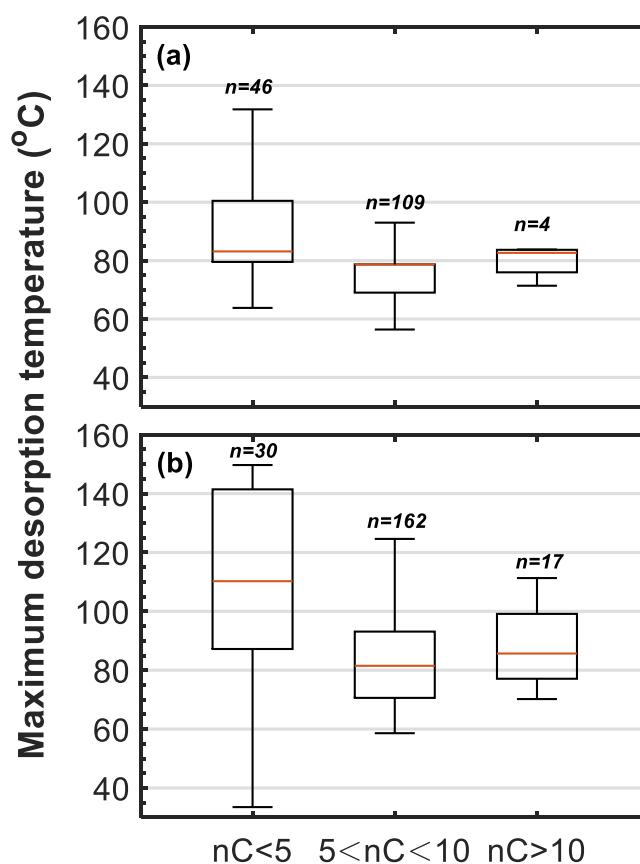
Figure 7: Boxplots of the maximum desorption temperatures of (a) the bulk products found in the mixed VOC system (i.e., unique products of _α_-pinene, _o_-cresol and common) and (b) products that were found unique in the mixed VOC system, weighted to their contribution to the total signal. Red lines represent the

530   **median values, each boxes' upper and lower limits represent the 75th and 25th percentile, respectively, while the errorbars represent the minimum and maximum values.**

4.2. Interpretation of FIGAERO-CIMS data

As has been shown here and elsewhere (e.g., Lopez-Hilfiker et al., 2016b;D'Ambro et al., 2017), linkages between the chemical composition and the particle volatility are possible using the FIGAERO-CIMS, while the individual product's volatility can be inferred qualitatively (Wang and Hildebrandt Ruiz, 2018) or quantitatively within an uncertainty (e.g., Bannan et al., 2019). Here we show for the first time that the technique can be used to distinguish the SOA products deriving from the oxidation of multiple precursors in environmental chambers, while being able to assess the potential role of product interactions in altering the SOA particle volatility. However, some limitations impact on results derived from the technique, such as the thermal desorption of the SOA collected in filters and the differential instrument sensitivity toward classes of compounds (Huang et al., 2018;Stark et al., 2017;Wang and Hildebrandt Ruiz, 2018;Lopez-Hilfiker et al., 2014).

We observed that the dominant o-cresol derived product, $C_7H_7NO_4$, exhibited different maximum desorption temperatures in the o-cresol single precursor experiments and the mixed VOC experiments (72.2 vs. 61.1 °C, respectively). This difference may result from differences in filter loadings between the experiments which were recently shown to affect the desorption profiles of the products due to matrix and/or saturation effects (Wang and Hildebrandt Ruiz, 2018;Ylisirniö et al., 2021). Expanding this to various characteristic products, we observe that their desorption profiles can have either a positive or negative relationship to the filter loading (Fig. S5). As also discussed in Schobesberger et al. (2018), a number of processes such as the thermal decomposition, isomerization, sample distribution in the filter and the uniformity of the heating may play a crucial role in the evaporation kinetics and parameters such as the enthalpy of vaporisation may have a determinant role in the shape of the thermograms. Consequently, comparing the desorption profiles of the products across systems with varying amounts of SOA formed and consequently filter loadings can be considered ambiguous. Here we qualitatively aim to establish the consistency of the overall shape of the sum thermograms with the volatility derived from independent quantitative techniques for the bulk of the SOA, but the quantitative retrieval of volatility distributions from the desorption temperature data is quite uncertain. A qualitative comparison of the shape of the maximum desorption temperature distributions may therefore be acceptable for the estimation of the bulk SOA particle volatility even when it is not possible to control filter loading.

Another characteristic of the CIMS technique is the varying instrument sensitivity toward different classes of compounds (Iyer et al., 2016;Lee et al., 2014). Recently, Hammes et al. (2019) showed that the sum of the 10

highest product signals accounted for ~50% of the acetate FIGAERO-CIMS signal in limonene photo-oxidation experiments. Here, in all the systems examined we also find that >45% of the total signal of the FIGAERO-CIMS can be attributed to the top 10 products (Fig. S6). Particularly, in the *o*-cresol experiments ~50% and ~40% of the total signal in the gas and particle phase respectively can be attributed to a single product ($C_7H_8O_2$ and $C_7H_7NO_4$,

565   respectively; Fig. S6). These results may indicate either that the aerosol composition is dominated by those few products or that the technique is overly sensitive to these compounds or a combination of both explanations.

The sum thermograms (defined as the sum of the individual ion thermograms), have been widely used to infer the volatility of the aerosols (e.g., Lopez-Hilfiker et al., 2015;D'Ambro et al., 2017;Huang et al., 2018;Lopez-Hilfiker et al., 2016b). However, a large fraction of the total signal is due to as few as 10 products (out of hundreds or

570   thousands typically found in the mass spectra) which in turn will largely define the shape of the sum thermogram (Fig. S7). Similarly, a number of studies have used various methods for estimating the saturation concentrations of the ions from CIMS data and expressed those results in the logarithmically spaced volatility bins as a function of their contribution to the total signal of the CIMS (e.g., Huang et al., 2019;Ylisirniö et al., 2020;Mohr et al., 2019;Tröstl et al., 2016). Conceivably, care should be taken in such an approach, since the major products will

575   have a determinant role at the resulting volatility distributions and may be related to the instrument used and the characteristics of each experiment, in turn resulting in a specific range of detected products.

Figure 3 shows that the sum thermogram of the *o*-cresol experiment is narrow owing to the dominant product accounting for 40% of the total particle phase signal. Meanwhile, the resultant volatility distributions from the TD measurements suggest wider volatility distribution in this system (Fig. 5). Figure 1 suggests that a large fraction of

580   the total particle phase signal of the FIGAERO-CIMS in the mixed VOC system is ostensibly related to *o*-cresol products (33%) with the signal from two products dominating this fraction ($C_7H_7NO_4$ =26% and $C_8H_{11}NO_3$=3%; Fig. S6). Therefore, caution should be exercised when attributing the contributions of individual precursor products to the mixed precursor products as the expression of FIGAERO-CIMS results in terms of the signal fraction can be misleading. Below we further explore the implications of the instrument sensitivity on our conclusions.

585   It is widely known that the I⁻-CIMS is highly sensitive to polar organic compounds with hydroxyl functional groups (Lee et al., 2014), while previously reported sensitivities resulting from calibrations of the I⁻-CIMS with various compounds showed to be spanning in orders of magnitude difference (Aljawhary et al., 2013). Iyer et al. (2016) using experimental data and preforming quantum calculations showed that the nitrogen as an element, and particularly if an ONO_2 group is added to a compound containing a hydroxyl group, had a substantial effect on the

590 I⁻-CIMS sensitivity. Particularly, the predicted and measured sensitivities of N-containing products investigated by Iyer et al. (2016) and Lee et al. (2014), respectively, might differ to up to two orders of magnitude compared to other compounds containing carboxylic and hydroxyl groups. Considering that *o*-cresol oxidation largely yields OH- containing products (Schwantes et al., 2017), in conjunction with the observed particularly high contributions of N-containing products to the total signal in all *o*-cresol-containing experiments (Fig. S8), it is likely that

595 differential sensitivity plays a role in this apparent dominance.

In order to assess this while taking account the above, we reduced the calibration factor of all N-containing products by a factor of 10 and 100 and we observed the changes in the sum thermograms, shown on Figure 8. Interestingly, the overall shape of the distribution is not substantially changing in either case, while we did not observe any substantial differences between the two sensitivity scenarios. Considering the broad agreement between the

600 volatility distributions derived from TD measurements with the shape of the sum thermograms derived from the FIGAERO, these results further suggest that regardless of the instrument sensitivity the latter can be used to qualitatively assess the particle volatility.
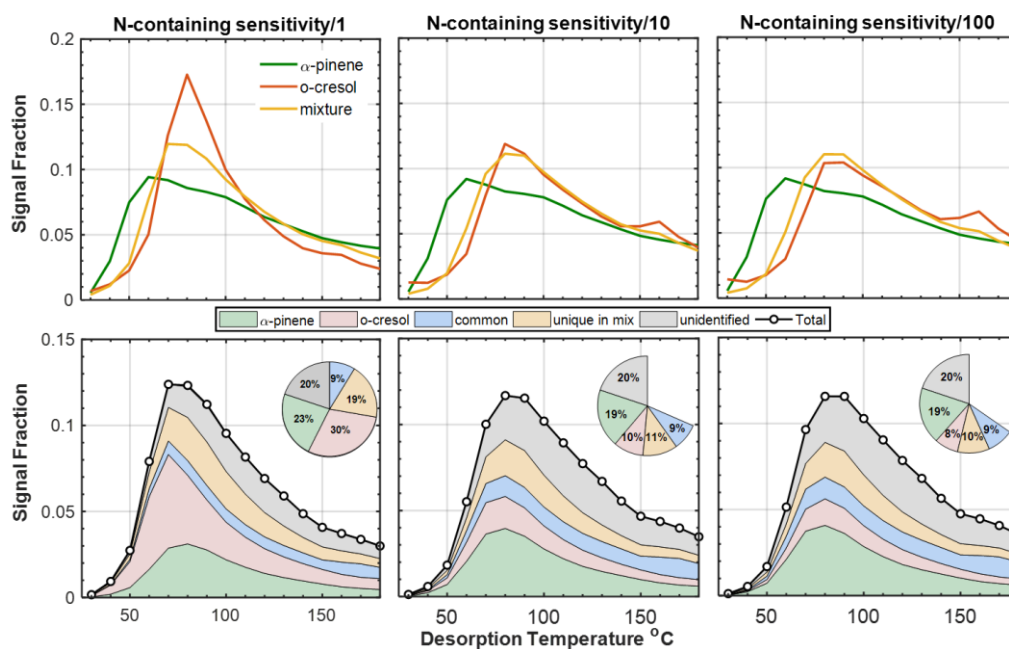
Figure 8: FIGAERO-CIMS sum thermograms for three characteristic experiments in each system (Exp. No.
605 **2, 5 and 10; Table 1) while varying the signal of the N-containing products (top panels) and corresponding**
sum thermogram from the mixed VOC experiment where the contributions of products that were associated

with either precursor, the common products, those that were found unique in the mixture, in addition the unidentified fractions are shown as areas (bottom panels). Inset pie charts are showing the contribution of each product class to the total signal. The missing fraction appearing the sensitivity scenarios is attributed

610   **to the fraction of the total signal that was reduced.**

It should be noted however, that the sensitivity effects could affect the linkage between the chemical composition and particle volatility. By altering the signal of N-containing products, we observe changes in the product distribution of the mixed VOC system. More specifically, the signal contribution of the unique *o*-cresol products

615   to the mixture reduces from 30 to 10%, assuming a reduction in the sensitivity of N-containing products by a factor of ten and then to 8% for a reduction of a factor of a hundred. Conversely, the respective reduction is much lower for the *α*-pinene products, which account 23% of the total signal assuming uniform sensitivity and 19% for both sensitivity scenarios. The signal fraction of the unique to the mix products is reduced roughly by half in both sensitivity scenarios compared to that assuming uniform sensitivity (19 to ~10%, respectively). The level of

620   reduction is associated well with the fraction of the signal corresponding to products with CHON elemental formula in each system, where *o*-cresol showed the highest values, followed by the mixed VOC and the *α*-pinene (71, 35 and 19%, respectively; Fig. S8a). Interestingly however, each system exhibited comparable number fraction of products containing C, H, O and N atoms (Fig. S8b), suggesting either that the nitrogen-containing oxidation products of *o*-cresol actually contribute substantially to the SOA mass and/or that there is a significant differential

625   sensitivity of the instrument towards molecules containing C, H, O and N. Because of the lack of information regarding the I$^-$-CIMS sensitivity towards aromatic and nitrogen-containing compounds, this cannot be directly investigated here but should be an area for future research.

However, further consideration of the increased SOA formation potential of *α*-pinene and the corresponding modest SOA yield of *o*-cresol (Fig. S9), might suggest that the domination of *o*-cresol products in the particle phase is

630   unlikely. Therefore taking into account:

i)   our observations in all the sensitivity scenarios examined showed that the unique to the mix products contribute considerably to the total signal (Fig. 1 and Fig. 8) and are of lower volatility than the average (Fig. 7);

ii)   in all sensitivity scenarios the products of *o*-cresol, which are of lower volatility (Fig. 3 and Fig.4), also contribute appreciably to the total signal;

635 iii) the products of α-pinene, whose products are likely contributing substantially to the SOA particle mass (both due to the large portion of the total signal and the increased nC; Fig. 1) and are of relatively higher volatility (Fig. 3 and Fig.4),

we can argue that the products of the higher yield precursor (i.e., α-pinene) may contribute substantially to the volatility of the mixture, while the contributions of the *o*-cresol products as well as those resulting from the mixing

640 of the precursors are lowering the overall volatility.

5. Conclusions

Many climate/air quality prediction models express SOA volatility based on single-precursor experiments and neglecting the potential interactions of the oxidation pathways of the different precursors leading to the SOA

645 formation (Yahya et al., 2017;Tsimpidi et al., 2018). However, more and more studies are showing that these results, obtained under simplified conditions and using single VOC precursor systems, might not represent accurately the ambient atmosphere in which hundreds of VOC are oxidized together (McFiggans et al., 2019;Shilling et al., 2019). Here, we investigate the SOA composition and volatility upon mixing characteristic anthropogenic and biogenic VOC precursors, using independent techniques.

650 Previously, Emanuelsson et al. (2013) observed an increase in the volume fraction remaining on SOA formed from the mixing various anthropogenic and biogenic precursors reacting sequentially. Here, we find the SOA particle volatility upon simultaneously mixing anthropogenic and biogenic precursors under initially iso-reactive mixing ratios appeared to be between the volatilities obtained in single precursor experiments. This is due to multiple processes taking place with some of them increasing the volatility, such as the scavenging of higher molecular

655 weight products, or decrease the volatility, such as the formation of new, more oxygenated and less volatile products.

There is some ambiguity in interpreting the FIGAERO-CIMS data owing to the different filter loadings as well as the a priori selectivity of the instrument towards certain products, defined by the instrument setup (Lee et al., 2014;Riva et al., 2019). In order to overcome these limitations, we have explored the impact of various scenarios

660 on the reported results and we show that the shape of the sum thermograms can be an acceptable qualitative measure of the SOA particle volatility. This was further confirmed by its broad agreement with the SOA particle volatility retrieved from an independent quantitative technique.

The results presented here call for further studies exploring the mechanisms that are driving these observations. Furthermore, the formation of new products in mixtures as well as the differential contribution of each precursor's
665   product to the particle phase implies a range of potential changes on the SOA properties and thereby their subsequent interactions with water vapour and other particles and gases (Champion et al., 2019;Riipinen et al., 2015;Pankow et al., 2015). Further, the potential effect of mixing anthropogenic and biogenic products might significantly affect the predicted SOA radiative forcing (Gordon et al., 2016;Kelly et al., 2018).

Data availability

670   All the data used in this work can be accessed on the open dataset of the EUROCHAMP programme (https://data.eurochamp.org/data-access/chamber-experiments/).

Acknowledgements

The Manchester Aerosol Chamber received funding from the European Union's Horizon 2020 research and innovation programme under grant agreement no. 730997, which supports the EUROCHAMP2020 research
675   programme. AV acknowledges the Presidents Doctoral Scholarship from the University of Manchester and the support from the Natural Environment Research Council (NERC) EAO Doctoral Training Partnership. MRA acknowledges funding support from the Natural Environment Research Council (NERC) through the UK National Centre for Atmospheric Science (NCAS). Instrumentational support was funded through the NERC Atmospheric Measurement and Observational Facility (AMOF).

680   **Competing interests**

The authors declare that they have no conflict of interest.

Author contributions

GM, MRA, AV, YW and YS conceived the study. AV, YW, YS and MD conducted the experiments. SNP provided the volatility retrieval algorithm. TJB provided on-site help deploying the FIGAERO-CIMS and discussing the
685   data analysis procedure. AV conducted the data analysis and wrote the manuscript with inputs from all co-authors.

References

Aiken, A. C., Salcedo, D., Cubison, M. J., Huffman, J. A., DeCarlo, P. F., Ulbrich, I. M., Docherty, K. S., Sueper, D., Kimmel, J. R., Worsnop, D. R., Trimborn, A., Northway, M., Stone, E. A., Schauer, J. J., Volkamer, R. M., Fortner, E., de Foy, B., Wang, J., Laskin, A., Shutthanandan, V., Zheng, J., Zhang, R., Gaffney, J., Marley, N. A., Paredes-Miranda, G., Arnott, W. P., Molina, L. T., Sosa, G., and Jimenez, J. L.: Mexico City aerosol analysis during MILAGRO using high resolution aerosol mass spectrometry at the urban supersite (T0) - Part 1: Fine particle composition and organic source apportionment, Atmospheric Chemistry and Physics, 9, 6633-6653, 10.5194/acp-9-6633-2009, 2009.

Alfarra, M. R., Hamilton, J. F., Wyche, K. P., Good, N., Ward, M. W., Carr, T., Barley, M. H., Monks, P. S., Jenkin, M. E., Lewis, A. C., and McFiggans, G. B.: The effect of photochemical ageing and initial precursor concentration on the composition and hygroscopic properties of beta-caryophyllene secondary organic aerosol, Atmospheric Chemistry and Physics, 12, 6417-6436, 10.5194/acp-12-6417-2012, 2012.

Aljawhary, D., Lee, A. K. Y., and Abbatt, J. P. D.: High-resolution chemical ionization mass spectrometry (ToF-CIMS): application to study SOA composition and processing, Atmos Meas Tech, 6, 3211-3224, 10.5194/amt-6-3211-2013, 2013.

Allan, J. D., Delia, A. E., Coe, H., Bower, K. N., Alfarra, M. R., Jimenez, J. L., Middlebrook, A. M., Drewnick, F., Onasch, T. B., Canagaratna, M. R., Jayne, J. T., and Worsnop, D. R.: A generalised method for the extraction of chemically resolved mass spectra from aerodyne aerosol mass spectrometer data, J Aerosol Sci, 35, 909-922, 10.1016/j.jaerosci.2004.02.007, 2004.

Atkinson, R.: Atmospheric chemistry of VOCs and NOx, Atmos Environ, 34, 2063-2101, https://doi.org/10.1016/S1352-2310(99)00460-4, 2000.

Baltensperger, U., Kalberer, M., Dommen, J., Paulsen, D., Alfarra, M. R., Coe, H., Fisseha, R., Gascho, A., Gysel, M., Nyeki, S., Sax, M., Steinbacher, M., Prevot, A. S. H., Sjogren, S., Weingartner, E., and Zenobi, R.: Secondary organic aerosols from anthropogenic and biogenic precursors, Faraday Discussions, 130, 265-278, 10.1039/b417367h, 2005.

Bannan, T. J., Le Breton, M., Priestley, M., Worrall, S. D., Bacak, A., Marsden, N. A., Mehra, A., Hammes, J., Hallquist, M., Alfarra, M. R., Krieger, U. K., Reid, J. P., Jayne, J., Robinson, W., McFiggans, G., Coe, H., Percival, C. J., and Topping, D.: A method for extracting calibrated volatility information from the FIGAERO-HR-ToF-CIMS and its experimental application, Atmos Meas Tech, 12, 1429-1439, 10.5194/amt-12-1429-2019, 2019.

Barley, M., Topping, D. O., Jenkin, M. E., and McFiggans, G.: Sensitivities of the absorptive partitioning model of secondary organic aerosol formation to the inclusion of water, Atmos. Chem. Phys., 9, 2919-2932, 10.5194/acp-9-2919-2009, 2009.

Bianchi, F., Kurten, T., Riva, M., Mohr, C., Rissanen, M. P., Roldin, P., Berndt, T., Crounse, J. D., Wennberg, P. O., Mentel, T. F., Wildt, J., Junninen, H., Jokinen, T., Kulmala, M., Worsnop, D. R., Thornton, J. A., Donahue, N., Kjaergaard, H. G., and Ehn, M.: Highly Oxygenated Organic Molecules (HOM) from Gas-Phase Autoxidation Involving Peroxy Radicals: A Key Contributor to Atmospheric Aerosol, Chem Rev, 119, 3472-3509, 10.1021/acs.chemrev.8b00395, 2019.

Brunekreef, B., and Holgate, S. T.: Air pollution and health, The Lancet, 360, 1233-1242, 10.1016/S0140-6736(02)11274-8, 2002.

725 Burkholder, J. B., Abbatt, J. P. D., Barnes, I., Roberts, J. M., Melamed, M. L., Ammann, M., Bertram, A. K., Cappa, C. D., Carlton, A. G., Carpenter, L. J., Crowley, J. N., Dubowski, Y., Georges, C., Heard, D. E., Herrmann, H., Keutsch, F. N., Kroll, J. H., McNeill, V. F., Ng, N. L., Nizkorodov, S. A., Orlando, J. J., Percival, C. J., Picquet-Varrault, B., Rudich, Y., Seakins, P. W., Surratt, J. D., Tanimoto, H., Thornton, J. A., Tong, Z., Tyndall, G. S., Wahner, A., Weschler, C. J., Wilson, K. R., and Ziemann, P. J.: The Essential Role for Laboratory Studies in 730 Atmospheric Chemistry, Environmental Science & Technology, 51, 2519-2528, 10.1021/acs.est.6b04947, 2017.

Cain, K. P., Karnezi, E., and Pandis, S. N.: Challenges in determining atmospheric organic aerosol volatility distributions using thermal evaporation techniques, Aerosol Sci Tech, 54, 941-957, 10.1080/02786826.2020.1748172, 2020.

Champion, W. M., Rothfuss, N. E., Petters, M. D., and Grieshop, A. P.: Volatility and Viscosity Are Correlated in 735 Terpene Secondary Organic Aerosol Formed in a Flow Reactor, Environ Sci Tech Let, 6, 513-519, 10.1021/acs.estlett.9b00412, 2019.

Chowdhury, P. H., He, Q. F., Male, T. L., Brune, W. H., Rudich, Y., and Pardo, M.: Exposure of Lung Epithelial Cells to Photochemically Aged Secondary Organic Aerosol Shows Increased Toxic Effects, Environ Sci Tech Let, 5, 424-430, 10.1021/acs.estlett.8b00256, 2018.

740 D'Ambro, E. L., Lee, B. H., Liu, J., Shilling, J. E., Gaston, C. J., Lopez-Hilfiker, F. D., Schobesberger, S., Zaveri, R. A., Mohr, C., Lutz, A., Zhang, Z., Gold, A., Surratt, J. D., Rivera-Rios, J. C., Keutsch, F. N., and Thornton, J. A.: Molecular composition and volatility of isoprene photochemical oxidation secondary organic aerosol under low- and high-NOx conditions, Atmos. Chem. Phys., 17, 159-174, 10.5194/acp-17-159-2017, 2017.

D'Ambro, E. L., Schobesberger, S., Gaston, C. J., Lopez-Hilfiker, F. D., Lee, B. H., Liu, J. M., Zelenyuk, A., Bell, 745 D., Cappa, C. D., Helgestad, T., Li, Z. Y., Guenther, A., Wang, J., Wise, M., Caylor, R., Surratt, J. D., Riedel, T., Hyttinen, N., Salo, V. T., Hasan, G., Kurten, T., Shilling, J. E., and Thornton, J. A.: Chamber-based insights into the factors controlling epoxydiol (IEPOX) secondary organic aerosol (SOA) yield, composition, and volatility, Atmospheric Chemistry and Physics, 19, 11253-11265, 10.5194/acp-19-11253-2019, 2019.

DeCarlo, P. F., Kimmel, J. R., Trimborn, A., Northway, M. J., Jayne, J. T., Aiken, A. C., Gonin, M., Fuhrer, K., 750 Horvath, T., Docherty, K. S., Worsnop, D. R., and Jimenez, J. L.: Field-deployable, high-resolution, time-of-flight aerosol mass spectrometer, Anal Chem, 78, 8281-8289, 10.1021/ac061249n, 2006.

Donahue, N. M., Robinson, A. L., Stanier, C. O., and Pandis, S. N.: Coupled partitioning, dilution, and chemical aging of semivolatile organics, Environmental Science & Technology, 40, 2635-2643, 2006.

Donahue, N. M., Kroll, J. H., Pandis, S. N., and Robinson, A. L.: A two-dimensional volatility basis set - Part 2: 755 Diagnostics of organic-aerosol evolution, Atmospheric Chemistry and Physics, 12, 615-634, 10.5194/acp-12-615-2012, 2012.

Eddingsaas, N. C., Loza, C. L., Yee, L. D., Chan, M., Schilling, K. A., Chhabra, P. S., Seinfeld, J. H., and Wennberg, P. O.: alpha-pinene photooxidation under controlled chemical conditions - Part 2: SOA yield and

composition in low- and high-NOx environments, Atmospheric Chemistry and Physics, 12, 7413-7427,
760 10.5194/acp-12-7413-2012, 2012a.

Eddingsaas, N. C., Loza, C. L., Yee, L. D., Seinfeld, J. H., and Wennberg, P. O.: alpha-pinene photooxidation
under controlled chemical conditions - Part 1: Gas-phase composition in low- and high-NOx environments,
Atmospheric Chemistry and Physics, 12, 6489-6504, 10.5194/acp-12-6489-2012, 2012b.

Emanuelsson, E. U., Hallquist, M., Kristensen, K., Glasius, M., Bohn, B., Fuchs, H., Kammer, B., Kiendler-Scharr,
765 A., Nehr, S., Rubach, F., Tillmann, R., Wahner, A., Wu, H. C., and Mentel, T. F.: Formation of anthropogenic
secondary organic aerosol (SOA) and its influence on biogenic SOA properties, Atmospheric Chemistry and
Physics, 13, 2837-2855, 10.5194/acp-13-2837-2013, 2013.

Farmer, D. K., Matsunaga, A., Docherty, K. S., Surratt, J. D., Seinfeld, J. H., Ziemann, P. J., and Jimenez, J. L.:
Response of an aerosol mass spectrometer to organonitrates and organosulfates and implications for atmospheric
770 chemistry, 107, 6670-6675, 10.1073/pnas.0912340107 %J Proceedings of the National Academy of Sciences,
2010.

Fuentes, E., and McFiggans, G.: A modeling approach to evaluate the uncertainty in estimating the evaporation
behaviour and volatility of organic aerosols, Atmos. Meas. Tech., 5, 735-757, 10.5194/amt-5-735-2012, 2012.

Garmash, O., Rissanen, M. P., Pullinen, I., Schmitt, S., Kausiala, O., Tillmann, R., Zhao, D., Percival, C., Bannan,
775 T. J., Priestley, M., Hallquist, Å. M., Kleist, E., Kiendler-Scharr, A., Hallquist, M., Berndt, T., McFiggans, G.,
Wildt, J., Mentel, T. F., and Ehn, M.: Multi-generation OH oxidation as a source for highly oxygenated organic
molecules from aromatics, Atmos. Chem. Phys., 20, 515-537, 10.5194/acp-20-515-2020, 2020.

Goldstein, A. H., and Galbally, I. E.: Known and unexplored organic constituents in the earth's atmosphere,
Environmental Science & Technology, 41, 1514-1521, 2007.

780 Gordon, H., Sengupta, K., Rap, A., Duplissy, J., Frege, C., Williamson, C., Heinritzi, M., Simon, M., Yan, C.,
Almeida, J., Trostl, J., Nieminen, T., Ortega, I. K., Wagner, R., Dunne, E. M., Adamov, A., Amorim, A.,
Bernhammer, A. K., Bianchi, F., Breitenlechner, M., Brilke, S., Chen, X. M., Craven, J. S., Dias, A., Ehrhart, S.,
Fischer, L., Flagan, R. C., Franchin, A., Fuchs, C., Guida, R., Hakala, J., Hoyle, C. R., Jokinen, T., Junninen, H.,
Kangasluoma, J., Kim, J., Kirkby, J., Krapf, M., Kurten, A., Laaksonen, A., Lehtipalo, K., Makhmutov, V., Mathot,
785 S., Molteni, U., Monks, S. A., Onnela, A., Perakyla, O., Piel, F., Petaja, T., Praplanh, A. P., Pringle, K. J., Richards,
N. A. D., Rissanen, M. P., Rondo, L., Sarnela, N., Schobesberger, S., Scott, C. E., Seinfeldo, J. H., Sharma, S.,
Sipila, M., Steiner, G., Stozhkov, Y., Stratmann, F., Tome, A., Virtanen, A., Vogel, A. L., Wagner, A. C., Wagner,
P. E., Weingartner, E., Wimmer, D., Winkler, P. M., Ye, P. L., Zhang, X., Hansel, A., Dommen, J., Donahue, N.
M., Worsnop, D. R., Baltensperger, U., Kulmala, M., Curtius, J., and Carslaw, K. S.: Reduced anthropogenic
790 aerosol radiative forcing caused by biogenic new particle formation, P Natl Acad Sci USA, 113, 12053-12058,
10.1073/pnas.1602360113, 2016.

Hallquist, M., Wenger, J. C., Baltensperger, U., Rudich, Y., Simpson, D., Claeys, M., Dommen, J., Donahue, N.
M., George, C., Goldstein, A. H., Hamilton, J. F., Herrmann, H., Hoffmann, T., Iinuma, Y., Jang, M., Jenkin, M.
E., Jimenez, J. L., Kiendler-Scharr, A., Maenhaut, W., McFiggans, G., Mentel, T. F., Monod, A., Prévôt, A. S. H.,
795 Seinfeld, J. H., Surratt, J. D., Szmigielski, R., and Wildt, J.: The formation, properties and impact of secondary
organic aerosol: current and emerging issues, Atmos. Chem. Phys., 9, 5155-5236, 10.5194/acp-9-5155-2009, 2009.

Hammes, J., Lutz, A., Mentel, T., Faxon, C., and Hallquist, M.: Carboxylic acids from limonene oxidation by ozone and hydroxyl radicals: insights into mechanisms derived using a FIGAERO-CIMS, Atmospheric Chemistry and Physics, 19, 13037-13052, 10.5194/acp-19-13037-2019, 2019.

800 Henry, F., Coeur-Tourneur, C., Ledoux, F., Tomas, A., and Menu, D.: Secondary organic aerosol formation from the gas phase reaction of hydroxyl radicals with m-, o- and p-cresol, Atmos Environ, 42, 3035-3045, 10.1016/j.atmosenv.2007.12.043, 2008.

Huang, W., Saathoff, H., Pajunoja, A., Shen, X., Naumann, K. H., Wagner, R., Virtanen, A., Leisner, T., and Mohr, C.: α-Pinene secondary organic aerosol at low temperature: chemical composition and implications for particle 805 viscosity, Atmos. Chem. Phys., 18, 2883-2898, 10.5194/acp-18-2883-2018, 2018.

Huang, W., Saathoff, H., Shen, X. L., Ramisetty, R., Leisner, T., and Mohr, C.: Seasonal characteristics of organic aerosol chemical composition and volatility in Stuttgart, Germany, Atmospheric Chemistry and Physics, 19, 11687-11700, 10.5194/acp-19-11687-2019, 2019.

Huffman, J. A., Docherty, K. S., Mohr, C., Cubison, M. J., Ulbrich, I. M., Ziemann, P. J., Onasch, T. B., and 810 Jimenez, J. L.: Chemically-Resolved Volatility Measurements of Organic Aerosol from Different Sources, Environmental Science & Technology, 43, 5351-5357, 10.1021/es803539d, 2009.

Isaacman-VanWertz, G., Massoli, P., O'Brien, R., Lim, C., Franklin, J. P., Moss, J. A., Hunter, J. F., Nowak, J. B., Canagaratna, M. R., Misztal, P. K., Arata, C., Roscioli, J. R., Herndon, S. T., Onasch, T. B., Lambe, A. T., Jayne, J. T., Su, L. P., Knopf, D. A., Goldstein, A. H., Worsnop, D. R., and Kroll, J. H.: Chemical evolution of atmospheric 815 organic carbon over multiple generations of oxidation, Nat Chem, 10, 462-468, 10.1038/s41557-018-0002-2, 2018.

Iyer, S., Lopez-Hilfiker, F., Lee, B. H., Thornton, J. A., and Kurten, T.: Modeling the Detection of Organic and Inorganic Compounds Using Iodide-Based Chemical Ionization, J Phys Chem A, 120, 576-587, 10.1021/acs.jpca.5b09837, 2016.

Jenkin, M. E., Saunders, S. M., Wagner, V., and Pilling, M. J.: Protocol for the development of the Master Chemical 820 Mechanism, MCM v3 (Part B): tropospheric degradation of aromatic volatile organic compounds, Atmospheric Chemistry and Physics, 3, 181-193, DOI 10.5194/acp-3-181-2003, 2003.

Jimenez, J. L., Jayne, J. T., Shi, Q., Kolb, C. E., Worsnop, D. R., Yourshaw, I., Seinfeld, J. H., Flagan, R. C., Zhang, X. F., Smith, K. A., Morris, J. W., and Davidovits, P.: Ambient aerosol sampling using the Aerodyne Aerosol Mass Spectrometer, J Geophys Res-Atmos, 108, Artn 8425

825 10.1029/2001jd001213, 2003.

Jimenez, J. L., Canagaratna, M. R., Donahue, N. M., Prevot, A. S. H., Zhang, Q., Kroll, J. H., DeCarlo, P. F., Allan, J. D., Coe, H., Ng, N. L., Aiken, A. C., Docherty, K. S., Ulbrich, I. M., Grieshop, A. P., Robinson, A. L., Duplissy, J., Smith, J. D., Wilson, K. R., Lanz, V. A., Hueglin, C., Sun, Y. L., Tian, J., Laaksonen, A., Raatikainen, T., Rautiainen, J., Vaattovaara, P., Ehn, M., Kulmala, M., Tomlinson, J. M., Collins, D. R., Cubison, M. J., Dunlea, E. 830 J., Huffman, J. A., Onasch, T. B., Alfarra, M. R., Williams, P. I., Bower, K., Kondo, Y., Schneider, J., Drewnick, F., Borrmann, S., Weimer, S., Demerjian, K., Salcedo, D., Cottrell, L., Griffin, R., Takami, A., Miyoshi, T., Hatakeyama, S., Shimono, A., Sun, J. Y., Zhang, Y. M., Dzepina, K., Kimmel, J. R., Sueper, D., Jayne, J. T.,

Herndon, S. C., Trimborn, A. M., Williams, L. R., Wood, E. C., Middlebrook, A. M., Kolb, C. E., Baltensperger, U., and Worsnop, D. R.: Evolution of Organic Aerosols in the Atmosphere, Science, 326, 1525-1529, 2009.

835 Jokinen, T., Sipilä, M., Richters, S., Kerminen, V.-M., Paasonen, P., Stratmann, F., Worsnop, D., Kulmala, M., Ehn, M., Herrmann, H., and Berndt, T.: Rapid Autoxidation Forms Highly Oxidized RO2 Radicals in the Atmosphere, 53, 14596-14600, https://doi.org/10.1002/anie.201408566, 2014.

Kanakidou, M., Seinfeld, J. H., Pandis, S. N., Barnes, I., Dentener, F. J., Facchini, M. C., Van Dingenen, R., Ervens, B., Nenes, A., Nielsen, C. J., Swietlicki, E., Putaud, J. P., Balkanski, Y., Fuzzi, S., Horth, J., Moortgat, G. K., 840 Winterhalter, R., Myhre, C. E. L., Tsigaridis, K., Vignati, E., Stephanou, E. G., and Wilson, J.: Organic aerosol and global climate modelling: a review, Atmos. Chem. Phys., 5, 1053-1123, 10.5194/acp-5-1053-2005, 2005.

Karnezi, E., Riipinen, I., and Pandis, S. N.: Measuring the atmospheric organic aerosol volatility distribution: a theoretical analysis, Atmos Meas Tech, 7, 2953-2965, 10.5194/amt-7-2953-2014, 2014.

Kelly, J. M., Doherty, R. M., O'Connor, F. M., and Mann, G. W.: The impact of biogenic, anthropogenic, and 845 biomass burning volatile organic compound emissions on regional and seasonal variations in secondary organic aerosol, Atmospheric Chemistry and Physics, 18, 7393-7422, 10.5194/acp-18-7393-2018, 2018.

Kramer, A. J., Rattanavaraha, W., Zhang, Z. F., Gold, A., Surratt, J. D., and Lin, Y. H.: Assessing the oxidative potential of isoprene-derived epoxides and secondary organic aerosol, Atmos Environ, 130, 211-218, 10.1016/j.atmosenv.2015.10.018, 2016.

850 Kristensen, K., Cui, T., Zhang, H., Gold, A., Glasius, M., and Surratt, J. D.: Dimers in alpha-pinene secondary organic aerosol: effect of hydroxyl radical, ozone, relative humidity and aerosol acidity, Atmospheric Chemistry and Physics, 14, 4201-4218, 10.5194/acp-14-4201-2014, 2014.

Kroll, J. H., and Seinfeld, J. H.: Chemistry of secondary organic aerosol: Formation and evolution of low-volatility organics in the atmosphere, Atmos Environ, 42, 3593-3624, 10.1016/j.atmosenv.2008.01.003, 2008.

855 Lee, A., Goldstein, A. H., Kroll, J. H., Ng, N. L., Varutbangkul, V., Flagan, R. C., and Seinfeld, J. H.: Gas-phase products and secondary aerosol yields from the photooxidation of 16 different terpenes, J Geophys Res-Atmos, 111, Artn D17305

10.1029/2006jd007050, 2006.

Lee, B. H., Lopez-Hilfiker, F. D., Mohr, C., Kurten, T., Worsnop, D. R., and Thornton, J. A.: An Iodide-Adduct 860 High-Resolution Time-of-Flight Chemical-Ionization Mass Spectrometer: Application to Atmospheric Inorganic and Organic Compounds, Environmental Science & Technology, 48, 6309-6317, 10.1021/es500362a, 2014.

Lelieveld, J., Evans, J. S., Fnais, M., Giannadaki, D., and Pozzer, A.: The contribution of outdoor air pollution sources to premature mortality on a global scale, Nature, 525, 367-+, 10.1038/nature15371, 2015.

Lopez-Hilfiker, F. D., Mohr, C., Ehn, M., Rubach, F., Kleist, E., Wildt, J., Mentel, T. F., Lutz, A., Hallquist, M., 865 Worsnop, D., and Thornton, J. A.: A novel method for online analysis of gas and particle composition: description and evaluation of a Filter Inlet for Gases and AEROsols (FIGAERO), Atmos Meas Tech, 7, 983-1001, 2014.

Lopez-Hilfiker, F. D., Mohr, C., Ehn, M., Rubach, F., Kleist, E., Wildt, J., Mentel, T. F., Carrasquillo, A. J., Daumit, K. E., Hunter, J. F., Kroll, J. H., Worsnop, D. R., and Thornton, J. A.: Phase partitioning and volatility of secondary organic aerosol components formed from alpha-pinene ozonolysis and OH oxidation: the importance of accretion products and other low volatility compounds, Atmospheric Chemistry and Physics, 15, 7765-7776, 10.5194/acp-15-7765-2015, 2015.

Lopez-Hilfiker, F. D., Iyer, S., Mohr, C., Lee, B. H., D'Ambro, E. L., Kurten, T., and Thornton, J. A.: Constraining the sensitivity of iodide adduct chemical ionization mass spectrometry to multifunctional organic molecules using the collision limit and thermodynamic stability of iodide ion adducts, Atmos Meas Tech, 9, 1505-1512, 10.5194/amt-9-1505-2016, 2016a.

Lopez-Hilfiker, F. D., Mohr, C., D'Ambro, E. L., Lutz, A., Riedel, T. P., Gaston, C. J., Iyer, S., Zhang, Z., Gold, A., Surratt, J. D., Lee, B. H., Kurten, T., Hu, W. W., Jimenez, J., Hallquist, M., and Thornton, J. A.: Molecular Composition and Volatility of Organic Aerosol in the Southeastern U.S.: Implications for IEPOX Derived SOA, Environmental Science & Technology, 50, 2200-2209, 10.1021/acs.est.5b04769, 2016b.

Louvaris, E. E., Karnezi, E., Kostenidou, E., Kaltsonoudis, C., and Pandis, S. N.: Estimation of the volatility distribution of organic aerosol combining thermodenuder and isothermal dilution measurements, Atmos Meas Tech, 10, 3909-3918, 10.5194/amt-10-3909-2017, 2017.

McFiggans, G., Artaxo, P., Baltensperger, U., Coe, H., Facchini, M. C., Feingold, G., Fuzzi, S., Gysel, M., Laaksonen, A., Lohmann, U., Mentel, T. F., Murphy, D. M., O'Dowd, C. D., Snider, J. R., and Weingartner, E.: The effect of physical and chemical aerosol properties on warm cloud droplet activation, Atmospheric Chemistry and Physics, 6, 2593-2649, DOI 10.5194/acp-6-2593-2006, 2006.

McFiggans, G., Topping, D. O., and Barley, M. H.: The sensitivity of secondary organic aerosol component partitioning to the predictions of component properties - Part 1: A systematic evaluation of some available estimation techniques, Atmospheric Chemistry and Physics, 10, 10255-10272, 10.5194/acp-10-10255-2010, 2010.

McFiggans, G., Mentel, T. F., Wildt, J., Pullinen, I., Kang, S., Kleist, E., Schmitt, S., Springer, M., Tillmann, R., Wu, C., Zhao, D., Hallquist, M., Faxon, C., Le Breton, M., Hallquist, Å. M., Simpson, D., Bergström, R., Jenkin, M. E., Ehn, M., Thornton, J. A., Alfarra, M. R., Bannan, T. J., Percival, C. J., Priestley, M., Topping, D., and Kiendler-Scharr, A.: Secondary organic aerosol reduced by mixture of atmospheric vapours, Nature, 565, 587-593, 10.1038/s41586-018-0871-y, 2019.

Mittal, L. A., Green, D. C., Sweeney, B. P., Quincey, P. G., and Fuller, G. W.: Sampling system influence on gaseous air pollution measurements, Atmos Environ, 79, 406-410, 10.1016/j.atmosenv.2013.06.051, 2013.

Mohr, C., Thornton, J. A., Heitto, A., Lopez-Hilfiker, F. D., Lutz, A., Riipinen, I., Hong, J., Donahue, N. M., Hallquist, M., Petäjä, T., Kulmala, M., and Yli-Juuti, T.: Molecular identification of organic vapors driving atmospheric nanoparticle growth, Nature Communications, 10, 4442, 10.1038/s41467-019-12473-2, 2019.

Moise, T., Flores, J. M., and Rudich, Y.: Optical Properties of Secondary Organic Aerosols and Their Changes by Chemical Processes, Chem Rev, 115, 4400-4439, 10.1021/cr5005259, 2015.

Olariu, R. I., Klotz, B., Barnes, I., Becker, K. H., and Mocanu, R.: FT-IR study of the ring-retaining products from the reaction of OH radicals with phenol, o-, m-, and p-cresol, Atmos Environ, 36, 3685-3697, Pii S1352-2310(02)00202-9

905   Doi 10.1016/S1352-2310(02)00202-9, 2002.

Pankow, J. F., Marks, M. C., Barsanti, K. C., Mahmud, A., Asher, W. E., Li, J. Y., Ying, Q., Jathar, S. H., and Kleeman, M. J.: Molecular view modeling of atmospheric organic particulate matter: Incorporating molecular structure and co-condensation of water, Atmos Environ, 122, 400-408, 10.1016/j.atmosenv.2015.10.001, 2015.

Priestley, M., Le Breton, M., Bannan, T. J., Leather, K. E., Bacak, A., Reyes-Villegas, E., De Vocht, F., Shallcross,
910   B. M. A., Brazier, T., Khan, M. A., Allan, J., Shallcross, D. E., Coe, H., and Percival, C. J.: Observations of isocyanate, Amide, Nitrate, and Nitro Compounds From an Anthropogenic biomass burning Using a Tof-CIMS, J Geophys Res-Atmos, 123, 7687-7704, 10.1002/2017jd027316, 2018.

Priestley, M., Bannan, T. J., Le Breton, M., Worrall, S. D., Kang, S., Pullinen, I., Schmitt, S., Tillmann, R., Kleist, E., Zhao, D., Wildt, J., Garmash, O., Mehra, A., Bacak, A., Shallcross, D. E., Kiendler-Scharr, A., Hallquist, Å.
915   M., Ehn, M., Coe, H., Percival, C. J., Hallquist, M., Mentel, T. F., and McFiggans, G.: Chemical characterisation of benzene oxidation products under high- and low-NOx conditions using chemical ionisation mass spectrometry, Atmos. Chem. Phys., 21, 3473-3490, 10.5194/acp-21-3473-2021, 2021.

Ramanathan, V., Crutzen, P. J., Kiehl, J. T., and Rosenfeld, D.: Atmosphere - Aerosols, climate, and the hydrological cycle, Science, 294, 2119-2124, DOI 10.1126/science.1064034, 2001.

920   Riipinen, I., Pierce, J. R., Donahue, N. M., and Pandis, S. N.: Equilibration time scales of organic aerosol inside thermodenuders: Evaporation kinetics versus thermodynamics, Atmos Environ, 44, 597-607, https://doi.org/10.1016/j.atmosenv.2009.11.022, 2010.

Riipinen, I., Rastak, N., and Pandis, S. N.: Connecting the solubility and CCN activation of complex organic aerosols: a theoretical study using solubility distributions, Atmospheric Chemistry and Physics, 15, 6305-6322,
925   10.5194/acp-15-6305-2015, 2015.

Rissanen, M. P., Kurtén, T., Sipilä, M., Thornton, J. A., Kangasluoma, J., Sarnela, N., Junninen, H., Jørgensen, S., Schallhart, S., Kajos, M. K., Taipale, R., Springer, M., Mentel, T. F., Ruuskanen, T., Petäjä, T., Worsnop, D. R., Kjaergaard, H. G., and Ehn, M.: The Formation of Highly Oxidized Multifunctional Products in the Ozonolysis of Cyclohexene, Journal of the American Chemical Society, 136, 15596-15606, 10.1021/ja507146s, 2014.

930   Riva, M., Rantala, P., Krechmer, J. E., Peräkylä, O., Zhang, Y., Heikkinen, L., Garmash, O., Yan, C., Kulmala, M., Worsnop, D., and Ehn, M.: Evaluating the performance of five different chemical ionization techniques for detecting gaseous oxygenated organic species, Atmos. Meas. Tech., 12, 2403-2421, 10.5194/amt-12-2403-2019, 2019.

Saha, P. K., and Grieshop, A. P.: Exploring Divergent Volatility Properties from Yield and Thermodenuder
935   Measurements of Secondary Organic Aerosol from alpha-Pinene Ozonolysis, Environmental Science & Technology, 50, 5740-5749, 10.1021/acs.est.6b00303, 2016.

Saunders, S. M., Jenkin, M. E., Derwent, R. G., and Pilling, M. J.: Protocol for the development of the Master Chemical Mechanism, MCM v3 (Part A): tropospheric degradation of non-aromatic volatile organic compounds, Atmospheric Chemistry and Physics, 3, 161-180, DOI 10.5194/acp-3-161-2003, 2003.

940   Schervish, M., and Donahue, N. M.: Peroxy radical chemistry and the volatility basis set, Atmos. Chem. Phys., 20, 1183-1199, 10.5194/acp-20-1183-2020, 2020.

Schobesberger, S., D'Ambro, E. L., Lopez-Hilfiker, F. D., Mohr, C., and Thornton, J. A.: A model framework to retrieve thermodynamic and kinetic properties of organic aerosol from composition-resolved thermal desorption measurements, Atmos. Chem. Phys., 18, 14757-14785, 10.5194/acp-18-14757-2018, 2018.

945   Schwantes, R. H., Schilling, K. A., McVay, R. C., Lignell, H., Coggon, M. M., Zhang, X., Wennberg, P. O., and Seinfeld, J. H.: Formation of highly oxygenated low-volatility products from cresol oxidation, Atmospheric Chemistry and Physics, 17, 3453-3474, 10.5194/acp-17-3453-2017, 2017.

Shilling, J. E., Zawadowicz, M. A., Liu, J. M., Zaveri, R. A., and Zelenyuk, A.: Photochemical Aging Alters Secondary Organic Aerosol Partitioning Behavior, Acs Earth Space Chem, 3, 2704-2716, 950   10.1021/acsearthspacechem.9b00248, 2019.

Shrivastava, M., Cappa, C. D., Fan, J. W., Goldstein, A. H., Guenther, A. B., Jimenez, J. L., Kuang, C., Laskin, A., Martin, S. T., Ng, N. L., Petaja, T., Pierce, J. R., Rasch, P. J., Roldin, P., Seinfeld, J. H., Shilling, J., Smith, J. N., Thornton, J. A., Volkamer, R., Wang, J., Worsnop, D. R., Zaveri, R. A., Zelenyuk, A., and Zhang, Q.: Recent advances in understanding secondary organic aerosol: Implications for global climate forcing, Rev Geophys, 55, 955   509-559, 10.1002/2016rg000540, 2017.

Spracklen, D. V., Jimenez, J. L., Carslaw, K. S., Worsnop, D. R., Evans, M. J., Mann, G. W., Zhang, Q., Canagaratna, M. R., Allan, J., Coe, H., McFiggans, G., Rap, A., and Forster, P.: Aerosol mass spectrometer constraint on the global secondary organic aerosol budget, Atmospheric Chemistry and Physics, 11, 12109-12136, 10.5194/acp-11-12109-2011, 2011.

960   Stark, H., Yatavelli, R. L. N., Thompson, S. L., Kimmel, J. R., Cubison, M. J., Chhabra, P. S., Canagaratna, M. R., Jayne, J. T., Worsnop, D. R., and Jimenez, J. L.: Methods to extract molecular and bulk chemical information from series of complex mass spectra with limited mass resolution, International Journal of Mass Spectrometry, 389, 26-38, https://doi.org/10.1016/j.ijms.2015.08.011, 2015.

Stark, H., Yatavelli, R. L. N., Thompson, S. L., Kang, H., Krechmer, J. E., Kimmel, J. R., Palm, B. B., Hu, W. W., 965   Hayes, P. L., Day, D. A., Campuzano-Jost, P., Canagaratna, M. R., Jayne, J. T., Worsnop, D. R., and Jimenez, J. L.: Impact of Thermal Decomposition on Thermal Desorption Instruments: Advantage of Thermogram Analysis for Quantifying Volatility Distributions of Organic Species, Environmental Science & Technology, 51, 8491-8500, 10.1021/acs.est.7b00160, 2017.

Stolzenburg, D., Fischer, L., Vogel, A. L., Heinritzi, M., Schervish, M., Simon, M., Wagner, A. C., Dada, L., 970   Ahonen, L. R., Amorim, A., Baccarini, A., Bauer, P. S., Baumgartner, B., Bergen, A., Bianchi, F., Breitenlechner, M., Brilke, S., Buenrostro Mazon, S., Chen, D., Dias, A., Draper, D. C., Duplissy, J., El Haddad, I., Finkenzeller, H., Frege, C., Fuchs, C., Garmash, O., Gordon, H., He, X., Helm, J., Hofbauer, V., Hoyle, C. R., Kim, C., Kirkby, J., Kontkanen, J., Kürten, A., Lampilahti, J., Lawler, M., Lehtipalo, K., Leiminger, M., Mai, H., Mathot, S.,

Mentler, B., Molteni, U., Nie, W., Nieminen, T., Nowak, J. B., Ojdanic, A., Onnela, A., Passananti, M., Petäjä, T.,
975   Quéléver, L. L. J., Rissanen, M. P., Sarnela, N., Schallhart, S., Tauber, C., Tomé, A., Wagner, R., Wang, M., Weitz,
L., Wimmer, D., Xiao, M., Yan, C., Ye, P., Zha, Q., Baltensperger, U., Curtius, J., Dommen, J., Flagan, R. C.,
Kulmala, M., Smith, J. N., Worsnop, D. R., Hansel, A., Donahue, N. M., and Winkler, P. M.: Rapid growth of
organic aerosol nanoparticles over a wide tropospheric temperature range, 115, 9122-9127,
10.1073/pnas.1807604115 %J Proceedings of the National Academy of Sciences, 2018.

980   Sulyok, M., Haberhauer-Troyer, C., and Rosenberg, E.: Observation of sorptive losses of volatile sulfur compounds
during natural gas sampling, J Chromatogr A, 946, 301-305, Doi 10.1016/S0021-9673(01)01541-2, 2002.

Topping, D. O., Barley, M. H., and McFiggans, G.: The sensitivity of Secondary Organic Aerosol component
partitioning to the predictions of component properties - Part 2: Determination of particle hygroscopicity and its
dependence on "apparent" volatility, Atmospheric Chemistry and Physics, 11, 7767-7779, 2011.

985   Tröstl, J., Chuang, W. K., Gordon, H., Heinritzi, M., Yan, C., Molteni, U., Ahlm, L., Frege, C., Bianchi, F., Wagner,
R., Simon, M., Lehtipalo, K., Williamson, C., Craven, J. S., Duplissy, J., Adamov, A., Almeida, J., Bernhammer,
A.-K., Breitenlechner, M., Brilke, S., Dias, A., Ehrhart, S., Flagan, R. C., Franchin, A., Fuchs, C., Guida, R., Gysel,
M., Hansel, A., Hoyle, C. R., Jokinen, T., Junninen, H., Kangasluoma, J., Keskinen, H., Kim, J., Krapf, M., Kürten,
A., Laaksonen, A., Lawler, M., Leiminger, M., Mathot, S., Möhler, O., Nieminen, T., Onnela, A., Petäjä, T., Piel,
990   F. M., Miettinen, P., Rissanen, M. P., Rondo, L., Sarnela, N., Schobesberger, S., Sengupta, K., Sipilä, M., Smith,
J. N., Steiner, G., Tomè, A., Virtanen, A., Wagner, A. C., Weingartner, E., Wimmer, D., Winkler, P. M., Ye, P.,
Carslaw, K. S., Curtius, J., Dommen, J., Kirkby, J., Kulmala, M., Riipinen, I., Worsnop, D. R., Donahue, N. M.,
and Baltensperger, U.: The role of low-volatility organic compounds in initial particle growth in the atmosphere,
Nature, 533, 527-531, 10.1038/nature18271, 2016.

995   Tsimpidi, A. P., Karydis, V. A., Pozzer, A., Pandis, S. N., and Lelieveld, J.: ORACLE 2-D (v2.0): an efficient
module to compute the volatility and oxygen content of organic aerosol with a global chemistry-climate model,
Geosci Model Dev, 11, 3369-3389, 10.5194/gmd-11-3369-2018, 2018.

Wang, D. S., and Hildebrandt Ruiz, L.: Chlorine-initiated oxidation of n-alkanes under high-NOx conditions:
insights into secondary organic aerosol composition and volatility using a FIGAERO–CIMS, Atmos. Chem. Phys.,
1000   18, 15535-15553, 10.5194/acp-18-15535-2018, 2018.

Wang, M., Chen, D., Xiao, M., Ye, Q., Stolzenburg, D., Hofbauer, V., Ye, P., Vogel, A. L., Mauldin, R. L.,
Amorim, A., Baccarini, A., Baumgartner, B., Brilke, S., Dada, L., Dias, A., Duplissy, J., Finkenzeller, H., Garmash,
O., He, X.-C., Hoyle, C. R., Kim, C., Kvashnin, A., Lehtipalo, K., Fischer, L., Molteni, U., Petäjä, T., Pospisilova,
V., Quéléver, L. L. J., Rissanen, M., Simon, M., Tauber, C., Tomé, A., Wagner, A. C., Weitz, L., Volkamer, R.,
1005   Winkler, P. M., Kirkby, J., Worsnop, D. R., Kulmala, M., Baltensperger, U., Dommen, J., El-Haddad, I., and
Donahue, N. M.: Photo-oxidation of Aromatic Hydrocarbons Produces Low-Volatility Organic Compounds,
Environmental Science & Technology, 54, 7911-7921, 10.1021/acs.est.0c02100, 2020.

Wyche, K. P., Monks, P. S., Ellis, A. M., Cordell, R. L., Parker, A. E., Whyte, C., Metzger, A., Dommen, J.,
Duplissy, J., Prevot, A. S. H., Baltensperger, U., Rickard, A. R., and Wulfert, F.: Gas phase precursors to
1010   anthropogenic secondary organic aerosol: detailed observations of 1,3,5-trimethylbenzene photooxidation,
Atmospheric Chemistry and Physics, 9, 635-665, DOI 10.5194/acp-9-635-2009, 2009.

Yahya, K., Glotfelty, T., Wang, K., Zhang, Y., and Nenes, A.: Modeling regional air quality and climate: improving organic aerosol and aerosol activation processes in WRF/Chem version 3.7.1, Geosci Model Dev, 10, 2333-2363, 10.5194/gmd-10-2333-2017, 2017.

1015   Yli-Juuti, T., Pajunoja, A., Tikkanen, O.-P., Buchholz, A., Faiola, C., Väisänen, O., Hao, L., Kari, E., Peräkylä, O., Garmash, O., Shiraiwa, M., Ehn, M., Lehtinen, K., and Virtanen, A.: Factors controlling the evaporation of secondary organic aerosol from α-pinene ozonolysis, 44, 2562-2570, https://doi.org/10.1002/2016GL072364, 2017.

Ylisirniö, A., Buchholz, A., Mohr, C., Li, Z., Barreira, L., Lambe, A., Faiola, C., Kari, E., Yli-Juuti, T., Nizkorodov,
1020   S. A., Worsnop, D. R., Virtanen, A., and Schobesberger, S.: Composition and volatility of secondary organic aerosol (SOA) formed from oxidation of real tree emissions compared to simplified volatile organic compound (VOC) systems, Atmos. Chem. Phys., 20, 5629-5644, 10.5194/acp-20-5629-2020, 2020.

Ylisirniö, A., Barreira, L. M. F., Pullinen, I., Buchholz, A., Jayne, J., Krechmer, J. E., Worsnop, D. R., Virtanen, A., and Schobesberger, S.: On the calibration of FIGAERO-ToF-CIMS: importance and impact of calibrant
1025   delivery for the particle-phase calibration, Atmos. Meas. Tech., 14, 355-367, 10.5194/amt-14-355-2021, 2021.

Zhang, X., Cappa, C. D., Jathar, S. H., Mcvay, R. C., Ensberg, J. J., Kleeman, M. J., and Seinfeld, J. H.: Influence of vapor wall loss in laboratory chambers on yields of secondary organic aerosol, P Natl Acad Sci USA, 111, 5802-5807, 10.1073/pnas.1404727111, 2014.

Zhang, X., McVay, R. C., Huang, D. D., Dalleska, N. F., Aumont, B., Flagan, R. C., and Seinfeld, J. H.: Formation
1030   and evolution of molecular products in α-pinene secondary organic aerosol, 112, 14168-14173, 10.1073/pnas.1517742112 %J Proceedings of the National Academy of Sciences, 2015.